



저작자표시-비영리-변경금지 2.0 대한민국

이용자는 아래의 조건을 따르는 경우에 한하여 자유롭게

- 이 저작물을 복제, 배포, 전송, 전시, 공연 및 방송할 수 있습니다.

다음과 같은 조건을 따라야 합니다:



저작자표시. 귀하는 원저작자를 표시하여야 합니다.



비영리. 귀하는 이 저작물을 영리 목적으로 이용할 수 없습니다.



변경금지. 귀하는 이 저작물을 개작, 변형 또는 가공할 수 없습니다.

- 귀하는, 이 저작물의 재이용이나 배포의 경우, 이 저작물에 적용된 이용허락조건을 명확하게 나타내어야 합니다.
- 저작권자로부터 별도의 허가를 받으면 이러한 조건들은 적용되지 않습니다.

저작권법에 따른 이용자의 권리는 위의 내용에 의하여 영향을 받지 않습니다.

이것은 [이용허락규약\(Legal Code\)](#)을 이해하기 쉽게 요약한 것입니다.

[Disclaimer](#)

Ph.D. Dissertation of Medicine

Cancer-associated fibroblast-
derived Fibulin-5 enhances
Epithelial-mesenchymal transition
in diffuse type gastric cancers via
c-AMP response element-binding
protein pathway

미만형 위암에서 암연관섬유아세포 유래
피블린5의 c-AMP 반응성 요소결합 단백질
경로를 통한 간엽상피전환 증가

August 2023

Graduate School of Medicine
Seoul National University
Internal Medicine

Jinju Choi

Cancer-associated fibroblast-
derived Fibulin-5 enhances
Epithelial-mesenchymal transition
in diffuse type gastric cancers via
c-AMP response element-binding
protein pathway

Sang Gyun Kim

Submitting a Ph.D. Dissertation of
Medicine

April 2023

Graduate School of Medicine
Seoul National University
Internal Medicine

Jinju Choi

Confirming the Ph.D. Dissertation written by
Jinju Choi
July 2023

Chair _____ (Seal)
Vice Chair _____ (Seal)
Examiner _____ (Seal)
Examiner _____ (Seal)
Examiner _____ (Seal)

Abstract

Diffuse-type gastric cancer (DGC) is comprised of small poorly cohesive cells with fibrotic stroma and is related to poor prognosis. Large-scale signaling network using three genomic databases of RNA-sequencing (TCGA, GSE62254, GSE26253) revealed *FBLN5* gene was highly activated in DGC compared with intestinal type and high *FBLN5* expression was associated with worse overall and disease specific survival in patients with DGC. Fibulin-5 was originated from cancer-associated fibroblasts (CAFs) in fibrotic stroma of DGC patient tissue, which promoted migration and epithelial-mesenchymal transition (EMT) expression of DGC cell line in co-culture system via downstream c-AMP-response element binding protein (CREB) pathway. Knock down of *FBLN5* attenuated the aggressive phenotype of DGC as well as CREB inhibitor treatment. In vivo experiment, xenograft tumors were more advanced in size, EMT and metastasis when DGC cells were engrafted with CAF and these aggressive features were decreased when co-engrafted CAFs were *FBLN5* knock down which can be a prognostic marker in patients with DGC.

Keyword : Diffuse gastric cancer, Cancer associated fibroblast, Fibulin-5, Epithelial-mesenchymal transition

Student Number : 2019-38342

Table of Contents

Chapter 1. Introduction.....	1
Chapter 1.1. Study Background.....	1
Chapter 1.2. Purpose of Research.....	3
Chapter 2. Body	4
Chapter 2.1. Materials and Methods.....	4
Chapter 2.2. Results	20
Chapter 2.3. Discussion.....	46
Chapter 3. Conclusion.....	49
Bibliography	50
Abstract in Korean	54
Supplements	55

Chapter 1. Introduction

1.1. Study Background

Gastric cancer is 5th most common cancer throughout all nations and ranked as 4th highest mortality among all cancers¹. In Korea, there is a national gastric cancer screening program by providing an upper GI endoscopy which is covered by national medical insurance, which affected the survival of gastric cancer by early detection of cancer. Furthermore, constant development of precision medicine for gastric cancer also contributed to the decrease of gastric cancer mortality in Korea². However, diffuse type which takes lower proportion of all gastric cancers but shows worse clinical outcome compared to intestinal type has not been fully understood although it maintains stable-to-increasing trend compared to the decreasing intestinal type gastric cancers³⁻⁶. Diffuse gastric cancer (DGC) is comprised of non-cohesive scattered tumor cells that lacks glandular structures and is surrounded by rich fibrotic stroma with abundant stromal cells including fibroblasts, immune cells in tumor microenvironment (TME)⁷⁻¹⁰. DGC is associated with epithelial mesenchymal transition (EMT) and abundant metastasis with unfavorable prognostic outcome and refractory to treatment¹¹. Unfortunately, the incidence of this aggressive phenotype of gastric cancer is increasing and understanding the pathophysiology and investigating the treatment strategy for this certain type of gastric cancer became an interest to physicians^{5,6,10}.

TME is comprised of diverse cells and extracellular matrix (ECM). TME has become rising research target because TME components dynamically interact with cancer cells, not only promotes tumor progression or metastasis, but also make resistance to anti-cancer treatment^{12,13}. In addition to the poorly cohesive nature of DGC, differentially expressed abnormal ECM molecules in DGC contributes to more invasion into adjacent tissue and aggressive distant metastasis via blood stream or lymphatic drainage which are related to poor survival and treatment outcome in DGC^{10,13-16}. Cancer-associated fibroblasts (CAFs) are most imperative and predominant cell components of TME that remodels stroma and interacts with cancer cell by secreting various cytokines and secretory proteins which promotes tumor cell proliferation, invasion and metastasis¹⁷⁻²⁰. There are many studies showing CAFs deposits matrix components and secretes various matrix remodeling proteins breaking the barrier and enables cancer cells to invade^{14,21,22}. CAFs also have pro-metastatic paracrine effect on cancer cells with growth factors, cytokines and exosomes to promote cancer invasion, metastasis and even resistance to treatment^{18,23-28}. Consequently, CAFs have been considered to be emerging potential target of anti-cancer therapy but it is still under investigation^{17,26}.

Fibulin-5 (FBLN5) is known for ECM glycoprotein related to elastic fiber components and is actively expressed during embryogenesis to differentiate the tissue and develop organs. When the development completes, activity of FBLN5 decrease but in the context of certain disease it is overexpressed resulting in increase

of ECM stiffness and fibrosis as well as the cell proliferation, migration and invasion²⁹⁻³¹. Previous studies investigating the role of FBLN5 on various human cancers including pancreatic, breast, lung, hepatocellular, ovarian and gastric cancers showed conflicting result according to clinical background^{29,32-41}. Specifying to gastric cancer, tendency of increased expression of fibulin-5 has been described but well-designed scientific report showing the mechanism or clinical implication is still insufficient⁴²⁻⁴⁵.

1.2. Purpose of Research

This study aimed to find out the biomarker which contributes the aggressiveness and worse prognosis of diffuse type gastric cancer compared to intestinal type followed by investigating the function of that marker.

Chapter 2. Body

2.1. Materials and Methods

2.1.1 Normalized equation modeling and numerical simulation

Based on the network topology, a normalized equation model describes the dynamics of each network component, the activity of which is constrained between 0 (minimum activity) and 1 (maximum activity). The configuration of differential equations differs depending on the number of incoming links to the node and the nature of the links (i.e., activation or inhibition). If one node (Y) is regulated by another node (X), the instantaneous rate of change in Y (dY/dt) is determined by the activity of X and the expression of Y (Supplemental Fig S1C (i), (ii)). When one node (Y) is regulated by the other two nodes (X and Z), the instantaneous rate of change in Y (dY/dt) is determined by the sum of the three influences: the individual influence of X on Y, the individual influence of Z on Y, and the expression of Y (Supplemental Fig. S1C (iii)). The equation includes four parameters, r_s , r_e , w_1 , w_2 : r_s represents the combined influence of X and Z on Y and r_e represents the influence of expression of Y on the activity of Y; w_1 represents the influence of X on Y and w_2 represents the influence on Z on Y. For simplicity, r_s , r_e were set to be 0.5 and weighting parameters were determined by 1 divided by the number of influencing nodes. In this

care, w_1 and w_2 were 0.5. If one node is regulated by the other three nodes, w_1 , w_2 , and w_3 will be 0.33.

Then, numerical simulations for the differential equation system were performed using `ode15s` function in MATLAB until stabilization under million random initial conditions. Since the simulation should be performed 1.1 billion times overall, the large-scale simulations were carried out by the high performance 64 core computer using parallel computation.

2.1.2 Mapping of RNA sequencing data to the signaling network

Information regarding causal relationship between various biological entities (i.e., mRNA, protein, phenotype, etc) for a large signaling network was collected from SIGNOR database (PMID: 26467481, signor.urinoma2.it). To minimize uncertainty inside a network, pre-processing of original database was conducted as follows: (1) remove links representing indirect/unknown effect, (2) remove links representing transcriptional regulation (since our model operates with pre-defined set of expression level), (3) remove nodes representing chemical, microRNA, fusion protein, phenotype, (4) remove duplicated links, (5) remove incoherent links (i.e., the link which represent activation and inhibition at the same time) assuming that the exact sign of the link is unknown, (6) remove links that activate/inhibit themselves (i.e., self-link).

RNA sequencing data from TCGA-STAD, GSE62254, and

GSE26253 datasets were acquired in the form of FPKM using R. To obtain RNA sequencing data from TCGA–STAD, R packages of TCGAWorkflowData, DT, TCGAbiolinks, httr, and jsonlite were used and to obtain those from GSE62254 and GSE26253, the GEOquery, Biobase, and limma packages were used. Then, by using ID mapping function provided by Uniprot, Ensemble gene identifier was converted into UniProtKB identifier. The assigned value of certain UniProtKB identifier was regarded as baseline gene expression of corresponding signaling component (www.uniprot.org). These values were mapped to the constructed signaling network, and the mapping rate (i.e., the fraction of nodes which have baseline expression values among all nodes belonging to the network) was 3131/3557, 3241/3557, and 2601/3557 in TCGA, GSE62254, and GSE26253, respectively. The baseline expression value of an unmapped node is assumed to be the average value of expressions of all nodes inside the network. Baseline expression values were normalized using z-score transformation and cumulative distribution functions (i.e, the lowest value is 0 and the highest value is 1) and used as a variable inside the normalized equation model.

2.1.3. Immunohistochemical analysis

Tissue microarray (TMA) blocks of 289 gastric cancers from surgical specimens of gastric cancer patients who underwent gastrectomy in Seoul National University Bundang Hospital

(SNUBH) between May 2006 and March 2012 were constructed using a tissue array device (Beecher Instruments Inc.). Review of consent for the use of surgical specimen for constructing TMA block was obtained from the patients and Institutional Review Board of SNUBH approved this study. Immunohistochemical (IHC) staining for fibulin-5 was performed on the TMA slides. For FBLN5, a rabbit polyclonal antibody HPA000868 (Atlas) was used at 1:50 dilution in 37°C incubation for 32 minutes. Other markers including BIRC5 (Rabbit monoclonal, ab76424, Abcam, 2.522mg/ml, 1:500), TTK (Mouse monoclonal, 35-9100, Thermo, 0.5mg/ml, 1:25), NEK2 (Mouse monoclonal, H00004751-M01, Abnova, 0.485mg/ml, 1:1000), FHL1 (Rabbit polyclonal, HPA001040, Atlas, 0.1mg/ml, 1:100), NR2F1 (Rabbit monoclonal, ab181137, Abcam, 0.485mg/ml, 1:400) were also stained.

IHC staining for tumor from xenograft mice model was done with Fibulin-5 (abcam, ab66339), Snail (NOVUS, NBP2-27293), p-CREB (abcam, ab32096) antibodies under the recommended condition by the instruction from the company.

2.1.4 Gene Set Enrichment Analysis (GSEA)

Public data sets for gastric cancer samples (n = 415) were collected from The Cancer Genome Atlas (TCGA) and subjected to gene set enrichment analysis (GSEA). Expressed genes were defined as the genes whose normalized read numbers for all samples were greater than 10. The top and bottom 10% of the

population selected by expression level of FBLN5 were defined as the FBLN5^{high} and FBLN5^{low} (n = 42 each), respectively. Differently expressed genes were defined as genes with fold change > 1.5 and p value <0.05 between two divided groups based on FBLN5 level. Genes were ordered according to their ranked ratios, and GSEA was performed using the GSEA tool (version 4.1.0). Gene lists of gene sets were based on the Human RT² Profiler PCR array (SABiosciences) and KEGG (Kyoto Encyclopedia of Genes and Genomes) Normalized enrichment score (NES) > 1.5, P-value < 0.05 and False Discovery Rate (FDR) < 0.25 was interpreted as statistically different. mRNA expression levels of each gene were normalized by the Z-score transformation and reported as a heatmap.

2.1.5 Single cell RNA sequencing

Fresh cancer tissue of diffuse gastric cancer patients with informed consent was taken by biopsy forcep during the endoscopic exam. The tissue was dissociated into single-cell suspensions using tumor dissociation kit, human (Miltenyi Biotec, Germany, #130-095-929) following the instructed dissociation protocols of the company. Samples with cell concentration > 5x10⁵/ml and cell viability > 70% passed in cellular quality control and loaded into 10x Genomics Chromium single cell 3' work system. Single cell RNA sequencing was done after generating Gel Bead in Emulsion (GEMs). Cell ranger program from 10x Genomics and Seurat v2.0 were used

in analysis. This process was approved by the institutional review board of SNUH (IRB No. 2003-127-1110) Adjusted p-value from Wilcoxon test between fibroblast_11 versus all the other cell clusters was 2.8×10^{-304} .

2.1.6 Patient-derived fibroblast isolation and culture

Gastric cancer tissue sample from tumor and normal tissue of distant resection margin were obtained from diffuse gastric cancer patients undergoing surgery at Seoul National University Hospital. This process was approved by the institutional review board of SNUH (IRB No. 2006-052-1131) Surgical specimen was reviewed by experienced pathologists and final pathology was reported in routine process. Obtained tissue samples were washed with phosphate-buffered saline with 5% penicillin and streptomycin. The tissues were dissected into 2 to 3mm squares with surgical scissors dipped in culture media and washed three times with PBS and placed in 6well plate with regular distance. The samples were covered with 22mm glass cover glasses (#HSU-0101060) and cultured in Dulbecco's modified Eagle's medium (GIBCO Life Technologies) supplemented with 10% FBS, 1% penicillin, and streptomycin. Fibroblasts were isolated from both GC tissues (CAFs) and paired normal tissues (normal-tissue-associated fibroblasts, NAFs) with outgrowth method. Isolated fibroblasts were maintained in Dulbecco's modified Eagle's medium (GIBCO Life Technologies) supplemented with 10% FBS, 1% penicillin, and

streptomycin. The phenotype of the isolated fibroblasts was confirmed by staining with fibroblast. All experiments were conducted with fibroblasts under 9 passages.

2.1.7. Real-time PCR

Total cellular RNA was extracted with QIAzol (QIAGEN) and PureLink RNA Mini Kit (#12183018A) (Invitrogen Life Technologies), and eluted in RNase-free water. The concentration of isolated RNA was measured by a Nanodrop 2000 spectrophotometer (Thermo Fisher Scientific) at 260 nm. The cDNAs used as template in RT-qPCR reactions were prepared using 1000 ng of total-RNA. The mRNA expression was evaluated by RT-qPCR using AMPIGENE qPCR Green Mix Hi-ROX(#ENZ-NUC-104) (Enzo) and normalized to GAPDH in each sample. For PCR, the amplification was conducted in a Step-one TM Real-time PCR (Applied Bioscience). All reactions were carried out in triplicate. A comparative threshold cycle (Δ CT) method was used for comparison with values expressed as $2^{-\Delta\Delta$ CT.

[Quantitative real-time PCR primer information]

FAP F: 5-TGTGCATTGTCTTACGCCCT-3 R: 5-
CCGATCAGGTGATAAGCCGT-3

S100A4 F: 5- CAGAACTAAAGGAGCTGCTGACC-3 R: 5-
CTTGGAAGTCCACCTCGTTGTC-3

PDGF α F: 5- GACTTTCGCCAAAGTGGAGGAG-3 R: 5-
AGCCACCGTGAGTTCAGAACGC-3

PDGF β F: 5- GAGATGCTGAGTGACCACTCGA-3 R: 5-
GTCATGTTTCAGGTCCAACCTCGG-3

Vimentin F: 5- AGGCAAAGCAGGAGTCCACTGA-3 R: 5-
ATCTGGCGTTCCAGGGACTCAT-3

α SMA F:5- CTATGCCTCTGGACGCACAACCT-3 R: 5-
CAGATCCAGACGCATGATGGCA-3

2.1.8. Western blot

The cells were lysed with RIPA Buffer (10X) #9806 (Cell signaling technology) with Proteinase inhibitors #P3100-001 (GenDEPOT) and Phosphatase inhibitors #P3200-001 (GenDEPOT). Equal amount of total proteins denatured with electrophoresis loading buffer for analysis by sodium sulfate polyacrylamide gel electrophoresis (SDS-PAGE). Separated proteins were transferred from the gel to polyvinylidene difluoride (PVDF) membranes (Merck Millipore, 0.45 μ m, #IPVH00010) and incubated with primary antibodies overnight at 4°C. The protein was visualized using a horseradish peroxidase-conjugated secondary antibody and ECL (Thermo fisher, #1859698, #1859701), ChemiDoc XRS+ System (Bio Rad).

[Antibody information for western blot]

Fibulin-5 (abcam, ab202977), b-actin (Sigma, A5228), E-Cadherin (BD, BD610181), N-Cadherin (BE, BD610920), Vimentin (Santa cruz, sc-7557), Snail (NOVUS, NBP2-27293), Slug (Cell signaling, #9585), FAP (Invitrogen, PA599313), p-RSK-1 (S380)

(abcam, ab32203), RSK (abcam, ab32526), HSP60 (Invitrogen, #MA3-013), pCREB(S133) (abcam, ab32096), CREB (abcam, ab32515), p-GSK-3a(S21) (Cell Signaling, #8452), GSK-3a (Cell Signaling, #4818), p-GSK-3b(S9) (Cell Signaling, #5558), GSK-3b (Cell Signaling, #12456).

2.1.9. Immunocytochemistry

Cells were seeded in 12-well plates. After 24h, cells were fixed in 4% formaldehyde for 10 minutes, followed by washing and pre-blocking. The cells were then incubated with antibodies against anti-Fibulin5 antibody (Abcam, Catalog No. ab66339), anti-FAP antibody (Cell Signaling Technology, Catalog No. 66562) to detect cancer associated fibroblast cells. After the washing steps, the cells were incubated with fluorescent-conjugated secondary antibody for 1 hour. DAPI was used for nuclear staining. Images were recorded by confocal microscopy (Leica STDE CW).

[Immunoblot and immunofluorescence staining antibody information]

*Antibodies

FBLN5 #ab66339

FAP #66562 (Cell Signaling Technology)

PDGF Receptor α #3174 (Cell Signaling Technology)

PDGF Receptor β #3169 (Cell Signaling Technology)

A-Smooth Muscle Actin #19245 (Cell Signaling Technology)

Vimentin #5741 (Cell Signaling Technology)

S100A4 #13018 (Cell Signaling Technology)

GAPDH (Santa Cruz)

E-cad

N-cad

Vimentin

Snail

Slug

Claudin-1

*Secondary antibody for western blot

Goat anti-Mouse IgG HRP conjugated secondary antibody #A90-116P (BETHYL)

Goat anti-Rabbit IgG HRP conjugated secondary antibody #A120-101P (BETHYL)

*Secondary antibody for immunofluorescence

Allophycocyanin, crosslinked, Goat anti-Mouse IgG secondary antibody #A865 (Invitrogen, Thermo Fisher Scientific)

*DAPI

VECTASHIELD Mounting Medium with DAPI #H-1200 (VECTOR)

2.1.10. Immunofluorescence

Immunofluorescence

Fibulin-5 (Invitrogen, PA5-106664), Vimentin (Santa cruz, sc-7557), FAP (Invitrogen, PA599313), PDGFa (Santa cruz, sc-338),

PDGFb (Santa cruz, sc-339), S100A4 (Invitrogen, Cat #MA5-31333), N-cadherin (BE, BD610920), Snail (NOVUS, NBP2-27293),

2.1.11. Establish of copGFP stable cell line

MKN45 and SNU668 cells were stably transduced with GFP lentiviral particles (Santa Cruz Biotechnology, sc-108084) following the manufacturer's protocol. Briefly, cells were cultured in 12-well plates in complete medium. After 24h, the medium was removed and substituted with opti-MEM containing polybrene (Santa Cruz Biotechnology, sc-134220) at a final concentration of 10 μ g/ml. Then, cells were infected by adding the sh-cop GFP lentiviral particles to the culture, mixed by swirling, and incubated 4 hours. After 4 hours, the medium was changed with fresh complete medium, and cells were cultured with puromycin selection with 1~10 μ g/ml. After puromycin selection, GFP-positive cells were sorted.

2.1.12. Knock-down of FBLN5 by transfection of si RNA

For small-interfering RNA (siRNA) transfection, TransIT-X2 Dynamic Delivery System (Mirus Bio, LLC) was used. All siRNA duplexes were synthesized by Bioneer. The sequences of Fibulin5-targeting siRNAs were synthesized as follows: Human, Sense: 5'-GGCAGAGAAUUUACAUGCGGCAAAAG-3' and Antisense: 5'-

UUUGCCGCAUGUAAAAUUCUCUGCCAU-3'

2.1.13. Invasion and Migration assay

The invasion capacity of cancer cells was determined using a 24-well plate, Transwell chambers with an 8- μ m pore size, and Matrigel (100 μ g/mL). Approximately 5x10⁴ MKN-45 cell line in 200 μ l of serum-free DMEM were plated in the upper chambers, and normal fibroblasts and cancer associated fibroblasts was plated to the lower chambers with 800 μ l of 10% FBS DMEM. After 48h, MKN-45 cells in the filters of upper chamber were fixed with methanol and they were visualized with microscope after hematoxylin and eosin (H&E) stain. Quantified migration rate was compared between cancer mono-culture system and each co-culture system with NAF or CAF.

2.1.14. Human phospho-kinase array

Protein phosphorylation was quantified using the proteome Proteome Profiler Human Phospho-Kinase array kit (ARY022B, R&D Systems) according to the manufacturer's instructions. Protein extracts were prepared from untreated MKN45 single and MKN45 co-cultured with human fibroblasts. MKN45 cells rinsed with ice cold PBS, and lysed at 4 $^{\circ}$ C for 30min in Lysis Buffer on the Proteome Profiler Human Phospho-Kinase Array Kit (R&D Systems). The phospho-kinase array membranes were blocked,

incubated equal amount of conditioned medium from MKN45 overnight at 4°C, and then incubated further with cocktails of biotinylated detection antibodies for 2h at room temperature. Signal was detected with the ECL (Thermo fisher, #1859698, #1859701) and the images obtained underwent quantification by densitometry with ImageJ to determine phospho-protein levels.

2.1.15. Live cell imaging

MKN-45 was seeded on 96 well plate of high content live cell imaging system (Operetta CLS, PerkinElmer, MA, US) and cultured for 96 hours with or without matrix cell which included NAF or CAF at a ratio of 5:1. Cancer cell proliferation was compared between mono-culture system and co-culture system by kinetic analysis. Cell image was obtained as digital phase contrast images every 30 minutes using 20x high NA objective. Cell growth was analyzed by Harmony® high-content analysis software. Migration speed ($\mu\text{m/s}$) was compared between different MKN45 groups including MKN-45 mono, MKN-45 plus NAF, MKN-45 plus CAF, MKN-45 plus CAF treated with si-Control and MKN-45 plus CAF treated with si-FBLN5.

2.1.16. Wound scratch assay

MKN-45 was seeded on 96-well microplate as mono-culture group and co-culture group. Cancer cells of co-culture group was

mixed with either NAF or CAF at a ratio of 5:1. WoundMaker™ (Essen Bioscience, Michigan, USA) was loaded above the microplate and scratch wounds were created. Initial images were obtained and follow-up images were taken every 24 hours using inverted phase contrast microscope. Cancer cell migration was compared between mono-cultured cells and co-cultured cell with the ratio of relative open area over cell area.

2.1.17. Chemicals and proteins

Chemicals and proteins

666-15 (Sigma, 5383410001) was used as a CREB inhibitor

Recombinant Human Fibulin-5 Protein, (CF R&D system, Catalog #: 9006-FB) was used as a secreted fibulin-5

2.1.18. Patient-derived gastric cancer organoid

Patient derived gastric cancer organoids were established according to previous study and the study was approved by the Institutional Review Board. 72

2.1.19. Mouse xenograft model of diffuse gastric cancer

All animal studies were conducted following the protocol of Institutional Animal Care and Use Committee in Columbia University Irving Medical Center. Six to eight-week-old male BALB/c nu/nu mice were used for xenograft. Tcon3944 gastric tumors in Atp-

4b-Cre; Cdh1fl/fl; LSL-KrasG12D; Trp53fl/fl; Rosa26LSLYFP/YFP triple conditional (Tcon) mice were generated and harvested as described in previous study⁷³. Murine xenograft models were made with subcutaneous injection of Tcon3944 gastric tumor cells into the right flank of the mice and some groups were co-injected with murine CAF which were transfected with sh.Scr or shFBLN5. Tumor volume was calculated as length x (width)² x 0.52, three times a week until the termination of animal study. After 3 weeks after tumor injection or at a time the tumor volume reaches up to 1cm³, mice were sacrificed. Metastatic cancer model was established with tail vein injection of Tcon3944 tumor cells were done with or without CAF transfected with S.Cr or shFBLN5. After sacrifice, number of metastatic tumor nodules in both lungs was counted.

2.1.20. Enzyme-linked immunosorbent assay (ELISA)

Process of ELISA using DGC patients' plasma was approved by the institutional review board of SNUH (IRB No. 2006-060-1112). Plasma samples of DGC patients who underwent gastrectomy surgery for DGC were taken before going to the surgery with informed consents.

2.1.21. Statistical analysis

Clinico-pathologic features (age, sex, cancer location, gross type,

WHO histologic classification, Lauren type, tumor size, TNM staging, presence of lymphatic/vascular/perineural invasion, follow up duration) and survival data of each patient included in TMA analysis were collected. Categorical variables of patients' clinical data were analyzed using chi square or Fisher's exact test. Continuous variables of patients' clinical data and quantitative data of in vitro experiments were expressed as mean \pm SD and analyzed using Student's t-test. Survival analysis was done by Kaplan-Meier analysis and cox-proportional hazards model. Statistical analyses were performed using SPSS version 26.0 (IBM Corporation, New York, US).

2.2. Results

2.2.1. Differently activated signaling components between two Lauren type gastric cancer in signaling network analysis using SIGNOR database

Using SIGNOR database, a network which consists of 3557 nodes and 8509 links showing various signaling pathways and cross-talks was constructed (Supplementary figure S1B). Normalized equations were made in accordance with each different types of signal relationships included in constructed network creating mathematical model (Supplemental figure S2C). Mathematical modeling allows comparison of RNA sequencing profile in various conditions to be easier by standardizing the values of state variables and parameters between 0 and 1 (the value 0 denotes minimal activity and the value 1 denotes maximal activity). The computer simulations of RNA sequencing profile from three large-scale patient databases (i.e., TCGA, GSE62254, GSE26253) were conducted by parallel computing technique (see methods for details). Total number of included patients was 1139 (407 from TCGA, 300 from GSE62254, 432 from GSE26253). Since simulation was performed under one million initial conditions for each patient's RNA sequencing profile, one million activity profiles for each signaling component were produced as a result which can be represented in the form of distribution (Supplementary figure S1D). Differentially activated signaling components (DASCs) between IGC and DGC were investigated in each database. As a result, 383, 228, and 32 DASCs

were found in TCGA, GSE62254, and GSE26253 respectively and six DASCs were in the intersection (Figure 1A). BIRC5, TTK, and NEK2 were predominantly activated in intestinal-type GC whereas FHL1, NR2F1, and FBLN5 were highly activated in diffuse-type GC (Figure 1A–B).

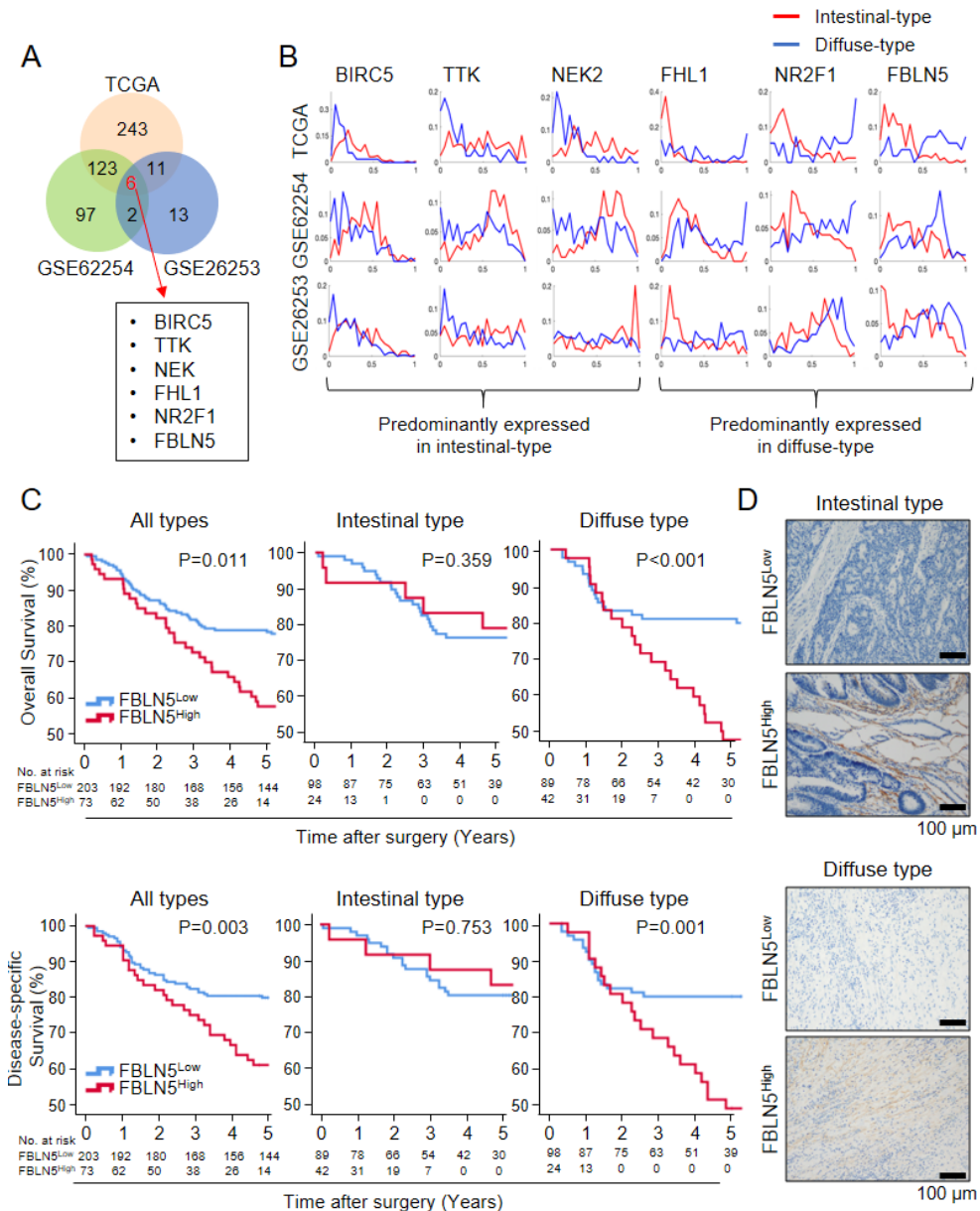


Figure 1. FBLN5 was one of differentially activated signaling components (DASC) between IGC and DGC, which was highly activated in DGC and has

worse prognostic (A) Six DASCs found by large scale network analysis in this study. (B) Activity distribution of the six DASCs in intestinal and diffuse type GCs. x-axis represents the scale of activity while y-axis is estimated density in distribution. Red line represents the density distribution of the signaling component in intestinal type GCs while blue line represents that in diffuse type GCs. (C) Kaplan-Meier curves for overall survival and disease-specific survival stratified by low vs high expression of FBLN5 in each Lauren types. (D) Representative immunohistochemical staining of FBLN^{Low} and FBLN^{High} cancer in each Lauren types. Scale bar 100µm.

2.2.2. High FBLN5 expression was correlated with worse survival outcome in diffuse gastric cancers included in the validation cohort

Tissue microarray (TMA) with tumor tissue from 277 gastric cancer patients who underwent surgical treatment with approachable clinic–pathologic features was performed for clinical validation of signaling network analysis described above. Expression level of previously described six markers was measured by the intensity x proportion of IHC staining of TMA blocks and it was compared between two Lauren types. (Table 1) Among six DASCs, two markers FBLN5 and TTK showed statistically significant difference of expression pattern between IGC and DGC which is compatible to signaling network analysis. High FBLN5 was predominant in DGC (IGC vs DGC 19.7% vs 32.1%, $p=0.031$) and high TTK expression in IGC (IGC vs DGC 15.6% vs 3.1%, $p=0.0001$). (Table 1–2)

To investigate the clinical significance of the markers, both overall survival and disease–specific survival were compared between patients with high or low expression of each six markers. All survival analyses were done in three different sets; all Lauren type GC, Intestinal type (IT), Diffuse type (DT) patient sets. (Supplementary figure S2A–E, S3A–E) In survival analysis, high expression of fibulin–5 was consistently associated with poor overall and disease–specific survival in all type and DT patient sets (Figure 1C). Other markers with statistical significance were as

follows. High TTK was associated with overall survival only in IT set ($p=0.035$) and low NR2F1 was related to worse overall and disease-specific survival in all type and IT analyses sets ($p=0.034$ for OS in all types, $p=0.001$ for DSS in all types, $p=0.013$ for OS in IT, $p=0.002$ for DSS in IT). (Supplementary figure S2A-E, S3A-E)

Among six DASCs, high activity or expression of FBLN5 in DGC was consistent in signal analysis and IHC stain in TMA blocks and significant survival difference was shown according to fibulin-5 expression level in survival analyses for both overall survival and disease-specific survival. (Figure 1D) Thus, we focused on FBLN5 among 6 DASCs. Difference of clinico-pathologic features of the patients according to the level of FBLN5 expression was evaluated including age, sex, tumor location, gross type, histology, tumor size, TNM stage, pathologic TN stage (Table 2). Cox-proportional hazard model was used to investigate the adjusted hazard ratio (HR) of overall and disease-specific mortality according to the level of FBLN5 expression. High expression of FBLN5 was related to increased risk of overall and diseases-specific mortality after adjustment of confounding variables including age, sex, location of tumor, tumor size, TNM stage (Adjusted HR for OS; 1.515, 95% CI; 1.019-2.251, $p=0.040$, Adjusted HR for DSS; 1.673, 95% CI; 1.013-2.762, $p=0.044$, Table 3-4).

Table 1. Expression levels of 6 proteins encoded by the six genes inferred from signaling network analyses according to the Lauren

type.

		Intestinal (n=122) n (%)	Diffuse (n=131) n (%)	P-value
BIRC5	High	112 (91.9%)	117 (89.3%)	0.528
	Low	10 (8.2%)	14 (10.7%)	
TTK	High	19 (15.6%)	4 (3.1%)	0.0001
	Low	103 (84.4%)	127 (96.9%)	
FHL1	High	30 (24.4%)	10 (7.6%)	<0.001
	Low	93 (75.6%)	121 (92.4%)	
NEK2	High	8 (6.6%)	5 (3.8%)	0.399
	Low	114 (93.4%)	126 (96.2%)	
NR2F1	High	61 (50.0%)	59 (45.0%)	0.452
	Low	61 (50.0%)	72 (55.0%)	
FBLN5	High	24 (19.7%)	42 (32.1%)	0.031
	Low	98 (80.3%)	89 (67.9%)	

Table 2. Comparison of baseline clinicopathologic features of two groups of gastric cancer patients divided by the expression level of FBLN5

	FBLN5 low	FBLN5 high	p-value
Age, years	61.39±11.4	56.40±11.3	0.001
Sex, N (%)			1.000
Male	127 (62.6%)	46 (63.0%)	
Female	76 (37.4%)	27 (37.0%)	
Location, N (%)			0.001
Lower third	102 (50.2%)	30 (41.1%)	
Middle third	74 (36.5%)	21 (28.8%)	
Upper third	26 (12.8%)	16 (21.9%)	
Entire	1 (0.5%)	6 (8.2%)	
Gross type, N (%)			0.127

Flat	16 (8.0%)	11 (15.7%)	
Protruded	34 (17.1%)	8 (11.4%)	
Depressed	149 (74.9%)	51 (72.9%)	
WHO classification, N (%)			0.103
TAWD	27 (13.3%)	9 (12.3%)	
TAMD	74 (36.5%)	15 (20.5%)	
TAPD	69 (34.0%)	36 (49.3%)	
SRC	27 (13.3%)	11 (15.1%)	
MAC	6 (3.0%)	2 (2.7%)	
Lauren type, N (%)			0.028
Intestinal	98 (48.3%)	24 (32.9%)	
Diffuse	105 (51.7%)	49 (67.1%)	
Tumor size (cm)	4.79±2.64	6.24±4.43	0.010
TNM stage, N (%)			0.02
Stage1–2	140 (69.0%)	36 (49.3%)	
Stage3–4	63 (31.0%)	37 (50.7%)	
Pathologic T stage, N (%)			0.002
pT1–2	126 (62.1%)	30 (41.1%)	
pT2–3	77 (37.9%)	43 (58.9%)	
Pathologic N stage, N (%)			0.221
pN0	101 (49.8%)	30 (41.1%)	
pN1–3	102 (50.2%)	43 (58.9%)	

Table 3. Cox–proportional hazards model for overall mortality adjusted by age, sex, location, tumor size, TNM stage, FBLN5 expression

	Univariable			Multivariable		
	HR	95%CI	p-value	HR	95%CI	p-value
Age	1.042	1.023–1.062	<0.001	1.053	1.033–1.073	<0.001
Sex						
Male	1 (ref)			1 (ref)		

Female	0.578	0.387–0.864	0.006	0.654	0.436–0.983	0.041
Location			<0.001			
Lower	1 (ref)					
Middle	0.621	0.398–0.968	0.035			
Upper	1.505	0.936–2.420	0.092			
Entire	6.772	3.048–15.043	<0.001			
Size	1.224	1.168–1.283	<0.001	1.176	1.106–1.250	<0.001
Gross						
Flat	1 (ref)		0.287			
Protruded	0.567	0.279–1.150	0.116			
Depressed	0.235	0.404–1.249	0.235			
Lauren						
Intestinal	1 (ref)		0.862			
Diffuse	1.075	0.738–1.565	0.705			
Mixed	1.182	0.601–2.325	0.628			
TNM						
Stage I	1 (ref)			1 (ref)		
≥ Stage II	3.745	2.502–5.605	<0.001	2.867	1.821–4.516	<0.001
FBLN5						
Low	1 (ref)			1 (ref)		
High	1.626	1.107–2.390	0.013	1.515	1.019–2.251	0.040

Table 4. Cox–proportional hazards model for disease–specific mortality adjusted by age, sex, location, gross type, lauren type, tumor size, TNM stage, FBLN5 expression

	Univariable			Multivariable		
	HR	95%CI	p–value	HR	95%CI	p–value
Age	1.007	0.986–1.028	0.531	1.026	1.004–1.049	0.021
Sex						
Male	1 (ref)			1 (ref)		
Female	0.629	0.375–1.057	0.080	0.590	0.344–1.012	0.055
Location			<0.001			
Lower	1 (ref)					
Middle	0.491	0.259–0.930	0.029			
Upper	1.698	0.949–3.041	0.075			
Entire	6.839	2.838–16.482	<0.001			

Gross				<0.001			
Flat	1 (ref)			0.037			
Protruded	0.310	0.120–0.801		0.016			
Depressed	0.535	0.278–1.028		0.060			
Size	1.251	1.190–1.316	<0.001	1.183	1.105–1.266	<0.001	
Lauren							
Intestinal	1 (ref)			0.041			
Diffuse	1.763	1.053–2.951		0.031			
Mixed	2.276	1.018–5.089		0.045			
TNM							
Stage I	1 (ref)				1 (ref)		
≥ Stage II	28.200	8.864–89.714	<0.001	17.668	5.437–57.418	<0.001	
FBLN5							
Low	1 (ref)				1 (ref)		
High	2.021	1.253–3.262	0.004	1.673	1.013–2.762	0.044	

2.2.3. FBLN5 is originated from cancer associated fibroblast abundant in cancer stroma

In the IHC staining result of TMA blocks shown above, stroma was strongly stained for fibulin-5 rather than cancer cells in TMA blocks. (Figure 1D) We further investigated the origin of fibulin-5 among stromal components by single cell RNA (scRNA) sequencing. (Figure 2A-2B). Fresh DGC tissue samples were collected from four actual DGC patients for scRNA and thirteen cell clusters were identified. FBLN-5 was predominantly expressed in cancer associated fibroblast (CAF), which is abundant in cancer stroma (Figure 2B). Fibroblasts were isolated from normal and cancer tissue of actual gastric cancer patients using outgrowth method which are named as normal associated fibroblast (NAF) and patient-derived cancer associated fibroblast (PD-CAF), respectively. Morphology of isolated NAF and PD-CAF were spindle shaped in electron microscopic image and Immunofluorescence (IF) staining for FBLN5 and CAF marker FAP, α -SMA was done to verify the isolated NAF and PD-CAF. (Figure 2B) Expression of active CAF marker FAP and FBLN5 was checked in each isolated fibroblasts and PD-CAF showed higher expression of both FAP and FBLN5 compared with NAF in both RT-PCR and westernblot. (Figure 2C-2D) With regard to primary tissue, fibulin-5 expression was higher in tumor tissue compared with normal tissue in western blot (Figure 2D) Immunofluorescence (IF) staining of paired normal and cancer tissue samples also showed

high expression of FBLN5 in cancer tissue while that of normal tissue was scant. Furthermore, CAF as origin of FBLN5 was reconfirmed in merged IF images (Figure 2E) In each Lauren type gastric cancers, cancer tissues could be sub-classified into FBLN5^{Low} and FBLN5^{High} cancer according to intensity of IHC staining using patient TMA tissue set and we further examined the clinical meaning of FBLN^{High} in gastric cancer, especially DGC which showed correlation with poor survival as shown in this study above. (Figure 1C–1D)

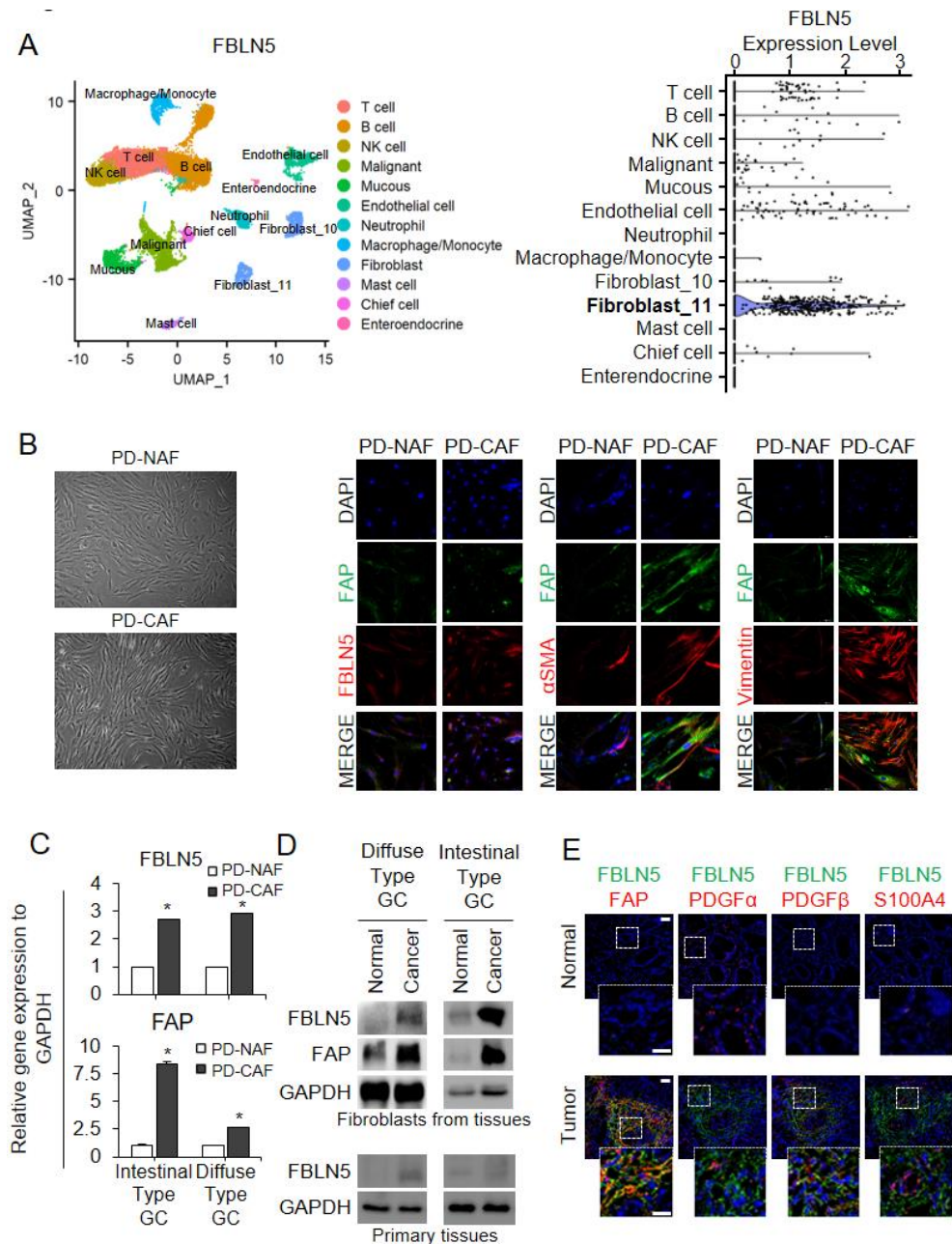


Figure 2. FBLN5 is derived from cancer-associated fibroblast (CAF) in cancer stroma (A) Single cell RNA sequencing with 4 diffuse gastric cancer patients to investigate the origin of FBLN5. Thirteen cell clusters were identified and shown as U map. Dot plot shows the expression level of FBLN5 in every cell clusters classified by scRNA sequencing and FBLN5 expression was highly expressed in CAF cluster. (B) Microscopic image of isolated fibroblast by outgrowth method in

each paired normal (NAF) and cancer tissue (CAF) of actual diffuse gastric cancer patients. Isolated NAF and CAF were verified by CAF markers and FBLN5 expression was checked by immunofluorescent staining. (C) Isolated fibroblasts from paired normal and cancer tissue showed higher FBLN5 mRNA expression in CAF compared to NAF in RTqPCR. (D) Fibulin-5 expression of primary cancer tissue was higher than that of normal tissue in both Lauren types in western blot. FAP expression was checked in isolated fibroblasts from paired normal and cancer tissue to verify the CAF by western blot. FBLN5 expression was high in CAF compared to NAF. (E) Immunofluorescent staining of paired patient normal and cancer tissue showed CAF markers and FBLN5 expression was high in tumor tissue. Merged image showed the site of FBLN5 expression overlapped with CAF marker expression. DAPI (blue), FBLN5 (green) and CAF markers (FAP, PDGF α , S100A4; red)

2.2.4. Fibulin-5 enhances epithelial-to-mesenchymal transition of diffuse gastric cancer cells.

Gene Set Enrichment Analysis (GSEA) was done to identify the differentially expressed genes between groups divided by FBLN5 expression level. Public data sets for gastric cancer samples (n = 415) were collected from The Cancer Genome Atlas (TCGA), which were subjected to the analysis. GSEA plots indicated significant enrichment of EMT in the FBLN5^{High} (n = 42) compared with FBLN5^{Low} patient groups (n = 42) (Figure 3A-3B). To investigate the possibility of the effect of CAF-derived fibulin-5 on DGC EMT, we adopted co-culture systems of prescreened DGC and CAF. (Supplementary figure S4A, S4C) Expression of fibulin-5 and vimentin of fibroblast was compared between fibroblast only

culture and fibroblast plus DGC cell lines (MKN-45, SNU668) by immunofluorescence staining. Fibulin-5 and vimentin of fibroblast were increased when cultured with DGC cell lines. (Figure 3C) Fibroblasts co-cultured with MKN-45 showed consistently increased expression of FBLN5 in western blot. (Figure 3D) Transfection of fibroblast with shFBLN5 effectively knockdown fibulin-5 expression of fibroblast in co-culture system evaluated by western blot. (Figure 3G) We compared cancer cell migration with or without CAF co-culture. Migration speed of MKN-45 was measured by live cell imaging analysis and it was enhanced when co-cultured with CAF and the effect slowed down after siFBLN5 treatment (Supplementary figure S4D, S4F). Wound scratch assay using live cell imaging system showed MKN-45 mixed with CAF showed improved closure of open wound area per cell area. (Figure 3E) To eliminate the effect of CAF migration, additional invasion and migration assay were done with transwell system. invasion and migration of DGC cell lines (MKN-45, SNU668) were also increased if they were co-cultured with CAF (Figure 3F, Supplementary figure S4E). MKN-45 and SNU668 co-cultured with CAF had increased expression of EMT markers (N-cadherin, vimentin, snail, slug) in western blots (Figure 3G) To prove the role of fibulin-5 in co-culture system, CAF was knockdown with sh*FBLN5* which was proven to be effectively transfected in prior to use and increasing effect of DGC cell line invasion and migration by co-culture was decreased. (Figure 3D, 3H, Supplementary figure S4B, S4G). The expression of EMT markers in DGC cell lines were

also decreased after FBLN5 knockdown in co-cultured CAF confirmed by western blot. (Figure 3I)

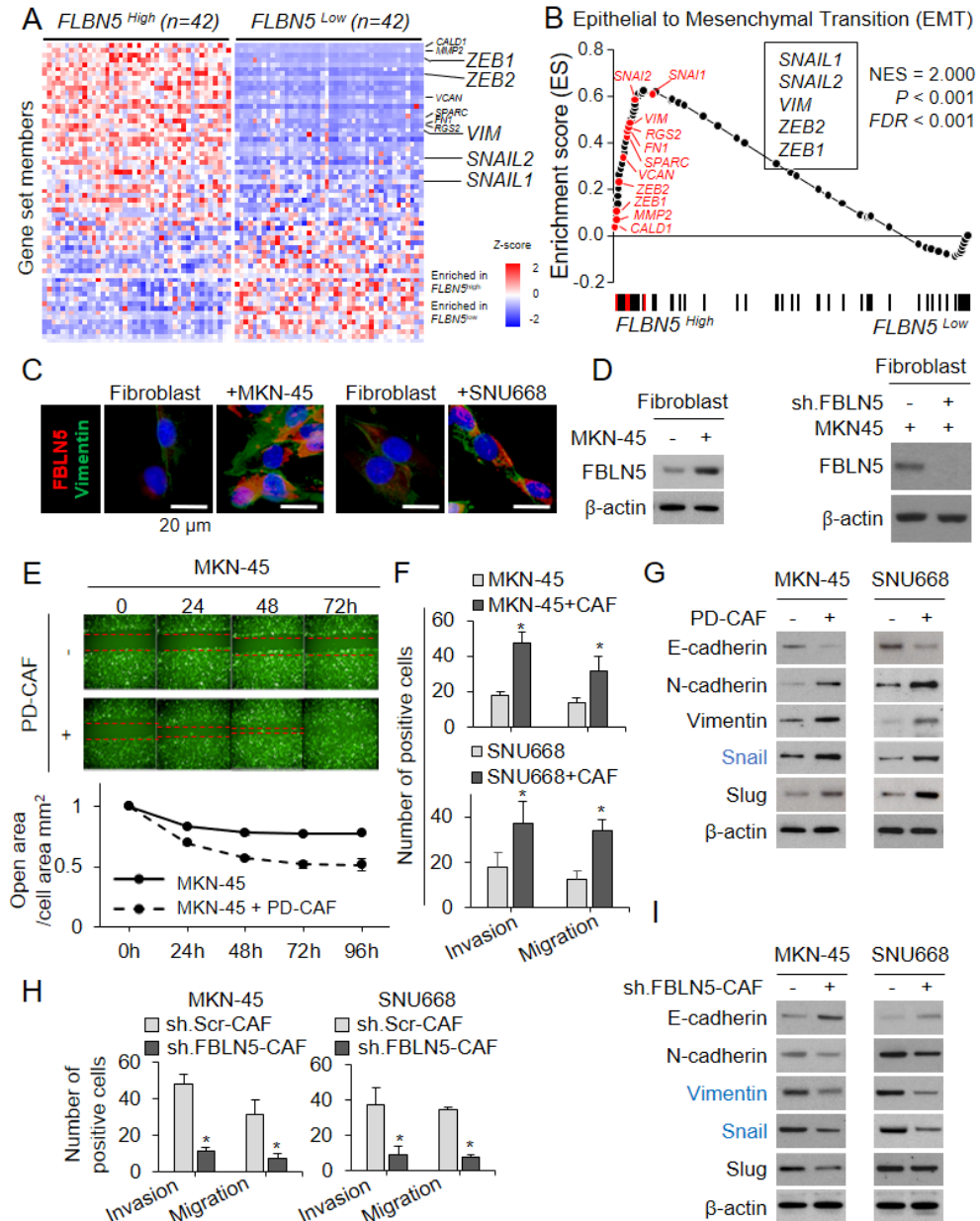


Figure 3. FBLN5 promotes Epithelial to Mesenchymal Transition (EMT) of DGC. (A) Heatmap from Gene Set Enrichment Analysis (GSEA) to investigate the gene set that shows different distribution between *FBLN5*^{Low} and *FBLN5*^{High}

patient groups. Colors are mRNA expression levels of each gene normalized by the Z-score transformation and expression of EMT gene set was significantly enriched in FBLN^{High} group compared to FBLN^{Low} group. (B) Enrichment score plot (black curve) from GSEA for ranked genes in EMT gene set. The normalized enrichment score (NES), nominal P-value, and False Discovery Ratio (FDR) are indicated. (C) Immunofluorescent staining for FBLN5 (red) and Vimentin (green) in fibroblast alone and fibroblast co-cultured with diffuse gastric cancer cell lines. Co-cultured fibroblast with cancer cell showed increased expression of vimentin and FBLN5 (D) Expression of FBLN5 increase in fibroblast when co-cultured with MKN-45 compared with that of fibroblast alone in western blot. Knockdown of FBLN5 expression was done effectively with the transfection of sh*FBLN5* in fibroblast co-cultured with MKN45. (E) Live cell imaging of and relative open wound area over cell area ratio captured at consecutive time points, compared between MKN45 mono-culture and co-culture with patient-derived cancer-associated fibroblast (PD-CAF). (E) Comparison of invasion and migration of diffuse gastric cancer (DGC) cell line (MKN45, SNU668) between cancer mono-culture system and co-culture system with cancer associated fibroblast (CAF) shown as bar graphs. (F) Western blot analysis for markers related to EMT. CAF co-culture with cancer cells decreased cancer E-cadherin expression whereas EMT marker expression was increased in MKN-45 and SNU668 when co-cultured with CAF. * $P < 0.05$ (G) Epithelial-mesenchymal transition (EMT) markers in DGC cell lines (MKN-45, SNU668) was increased in co-culture system cultured with PD-CAF compared with cancer mono-culture system. (H) Comparison of invasion and migration of DGC cell lines (MKN-45, SNU668) in cancer plus CAF co-culture system according to transfection of sh*FBLN5*. * $P < 0.05$. (I) EMT expression change in

cancer plus CAF co-culture system after FBLN5 was knockdown in CAF compared with shC treatment in CAF.

2.2.5. Fibulin-5 is secreted from CAF and can be detectable even in DGC patient plasma samples in higher concentration than normal patients.

To investigate how fibulin-5 from CAF acts on DGC, culture media of MKN-45 and CAF co-culture system was isolated and we quantified relative intensity of fibulin-5 expression by ELISA. Culture media isolated from co-culture system showed significantly high concentrations of fibulin-5 compared with culture media from cancer cell mono-culture system. (Figure 4A) Meanwhile, culture media from co-culture system which included FBLN5 knockdown CAF with DGC cell lines (MKN45, SNU668) showed marked decrease of fibulin-5. (Figure4B) This supports the paracrine effect of CAF on DGC as it secretes fibulin-5 in TME. To investigate possible systemic effect of fibulin-5 in addition to local effect in TME, DGC patients' blood samples were collected with informed consents and fibulin-5 concentration was measured using ELISA. Plasma sample of DGC showed significantly higher concentration of fibulin-5 compared with normal tissues of non-cancer disease patients. (Figure 4C, Supplementary figure S5B) Matched stomach tissue samples from the patients who provided blood samples for fibulin-5 ELISA were stained for FBLN5 and tissues from DGC patients showed higher H-score than normal

tissues consistent with plasma result. (Figure 4D) Positive correlation was found between plasma FBLN5 level and H-score for FBLN5 in stomach tissue ($R=0.671$, $P=0.034$) (Figure 4E)

Investigation of the effect of fibulin-5 on patient-derived DGC organoid was done in addition to the prior cell studies. Study result with organoids which share more similar features of patients' tumors than cells also supported promoting effect of CAF derived fibulin-5 on DGC. Paired bright-field image and H&E staining of patient-derived gastric cancer organoid (PD-GCO) were compared between two co-culture systems of PD-GCO and CAF, which can be divided by transfection of either Scr or sh*FBLN5* in CAF included in co-culture system. When it comes to co-culture system of PD-GCO with CAF which was transfected with sh*FBLN5* the number of organoids was markedly decreased. (Supplementary figure S5A, S5C) Number of organoids with size $>50\mu\text{m}$ were compared to see the effect of CAF co-culture or FBLN5 knockdown CAF co-culture on PD-GCOs. PD-GCOs which were co-cultured with CAF had increased number of organoids with size $>50\mu\text{m}$ but when it comes to FBLN5 knockdown PD-CAF, the increase didn't occur. (Figure 4F) Recombinant fibulin-5 was treated to mimic the paracrine effect of CAF on PD-GCO and the number of organoids with size $>50\mu\text{m}$ was significantly increased compared with untreated solitary PD-GCO. (Figure 4G)

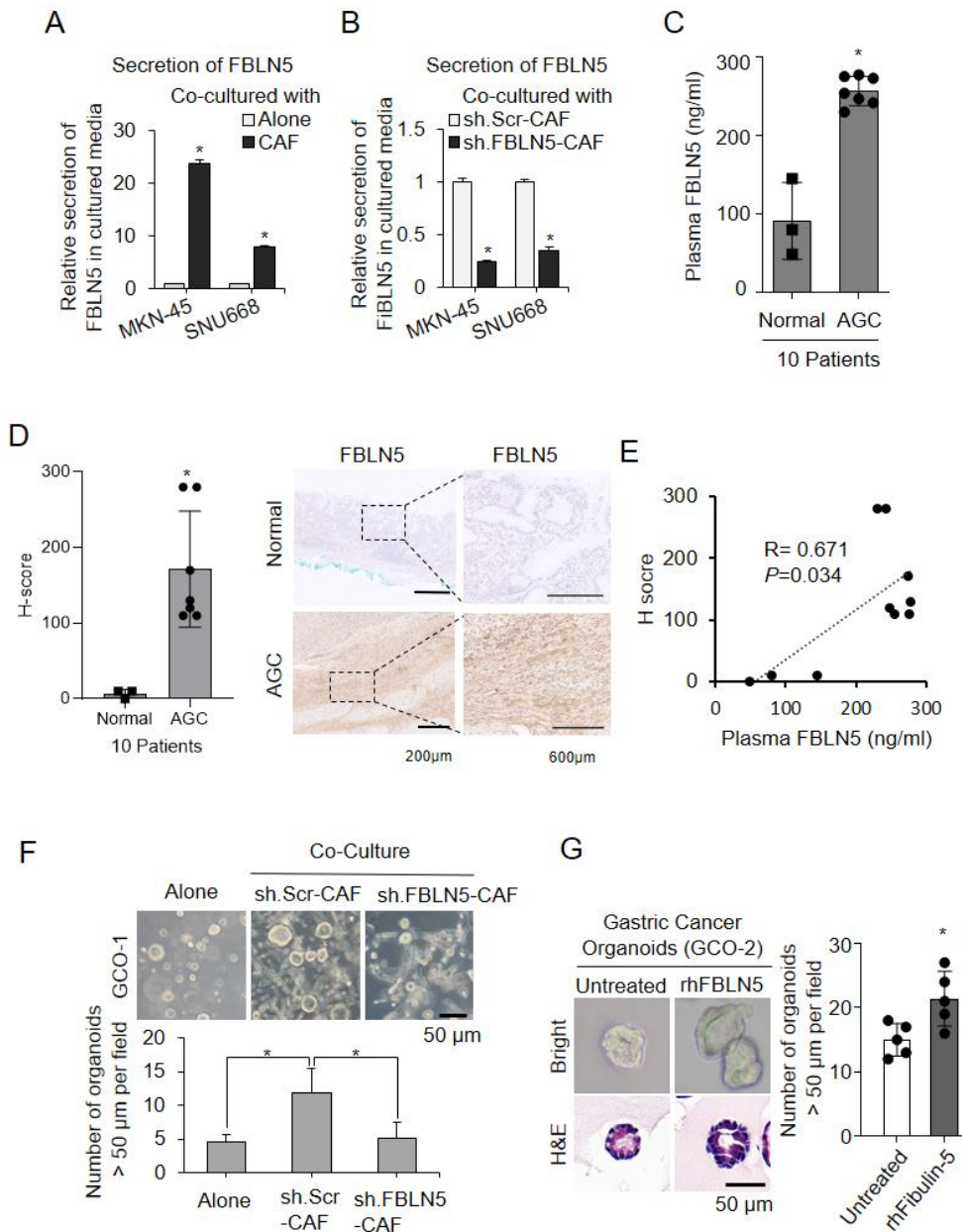


Figure 4. Fibulin-5 is secreted from CAF, which can be even detected in patients' plasma showing potential systemic effect and the local effect of fibulin-5 was examined in patient derived gastric cancer organoid (GCO) (A) Relative concentration of secreted fibulin-5 in culture media was compared between two culture systems which are cancer (MKN45, SNU668) mono-culture system and cancer plus CAF co-culture system. (B) Change of relative concentration of fibulin-5 in culture media from cancer plus CAF co-culture

system according to the transfection with *shFBLN5* to knockdown FBLN5 in CAF. (C) Concentration of plasma fibulin-5 (ng/mL) compared between actual non-cancer patients and diffuse gastric cancer patients measured by ELISA (D) Average H-score measured from FBLN5 IHC stain of non-cancer and advanced gastric cancer (AGC) patients. Representative IHC staining images for FBLN5 comparing non-cancer and AGC patient tissues. (E) Pearson's correlation coefficient and scatter plot between H-score from tumor tissue and plasma FBLN5 concentration of the patients. (F) Paired bright-field microscopy and H&E staining comparing between patient-derived diffuse GCOs co-cultured with CAF transfected with *shScr* or *shFBLN5*. Scale bar 50 μ m (G) Paired bright-field microscopy and H&E staining comparing between patient-derived diffuse GCOs treated with or without recombinant human fibulin-5 (rhFBLN5, 2 μ m/mL). Number of organoids with size greater than 50 μ m was counted in each groups divided by the treatment of rhFibulin-5 shown in bar graphs. Scale bar 50 μ m. * $P < 0.05$.

2.2.6. Fibulin-5 promotes epithelial-mesenchymal transition in DGC via c-AMP response element binding protein (CREB) pathway

To investigate the mediators included in signaling pathway of fibulin-5, phosphorylation profile of protein kinases was compared between MKN-45 mono-culture system and co-culture system with PD-CAF. Co-culture of MKN-45 with PD-CAF enforced phosphorylation of CREB, GSK3 α β , RSK1/2/3, HSP60 in cancer cells by phosphokinase array (Figure 5A-B). Increased expression of pCREB, pGSK3 α and pRSK1/2/3 in DGC cell lines (MKN-45, SNU668) co-cultured with CAF was shown consistently in western blot. (Figure 5C, Supplementary figure S6A) Treatment with sh-

FBLN5 in CAF reversed the increased phosphorylation of pCREB and pGSK3 α (Figure 5D). Regarding to these results we presumed CREB–GSK pathway could be a downstream signaling pathway of fibulin–5 regulating EMT in DGC. IF staining result showed that CREB knockdown in DGC consequently decreased the expression of EMT markers in DGC (Figure 5E). In western blot analysis, when CREB was inhibited either by sh*CREB* or CREB inhibitor 666–15 in co–culture system, CREB , GSK3 α and EMT markers (vimentin, snail, slug) of MKN45 and SNU668 were consequently decreased in co–culture system (Figure 5F, Supplementary figure S6B–C) CREB inhibition using shCREB or 666–15 also decreased invasion and migration of MKN45 and SNU668 in co–culture system (Figure 5G, Supplementary figure S6D–E) Immunofluorescence staining of PD–GCO showed treatment with recombinant human FBLN5 or CAF co–culture increased p–CREB in PD–GCO (Figure 5H–I)

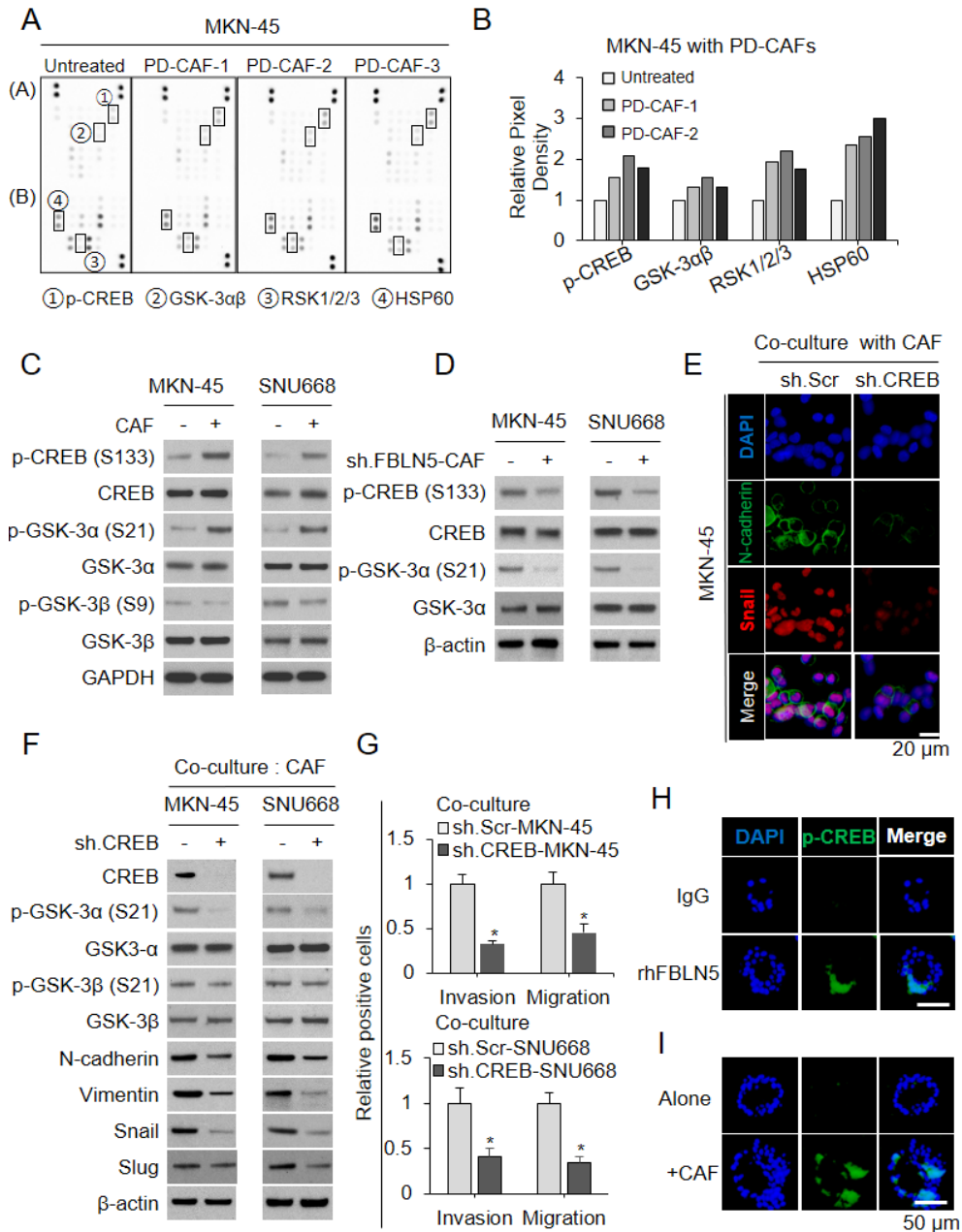


Figure 5. CAF-derived fibulin-5 increases cancer aggressiveness via cAMP

Response Element Binding Protein (CREB)

(A) Screening phosphokinase array to investigate the kinase pathway related to the downstream signal of fibulin-5 on gastric cancer cells. Signaling components which showed difference in MKN-45 according to the presence of patient-derived CAF (PD-CAF) were investigated. (B)

Bar graph shows relative quantitative change in pixel density of four kinases (p-CREB, GSK-3 α β , RSK 1/2/3, HSP60) that were significantly altered in MKN-45 co-culture system with PD-CAF compared with MKN-45 monoculture in phosphokinase array. (C) Comparison of the expression of components included in CREB-GSK pathway between diffuse gastric cancer (DGC) cell lines (MKN-45, SNU668) monoculture and co-culture with CAF by western blot. (D) Western blots to examine the suppression of CREB (pCREB Ser133) and GSK-3 α (pGSK-3 α Ser21) in DGC cell lines following the knockdown of FBLN5 in CAFs consisting of co-culture system. (E) Immunofluorescence (IF) staining image comparing co-culture system comprised of CAF and MKN-45 divided by MKN-45 transfection status either with shSCr or sh*CREB*. DAPI (blue), N-cadherin (green), Snail (red), Scale bar 20 μ m (F) Expression of CREB-GSK signal components and EMT markers (N-cadherin, Vimentin, Snail, Slug) compared between two co-culture system of each MKN45 or SNU668 with CAF divided by the transfection of sh*CREB* in cancer cell line. (G) Comparison of invasion and migration of DGC cell lines in CAF co-culture system comprised of either shSCr treated DGC cell line or sh*CREB* treated DGC cell line. (H) IF staining to investigate the difference of p-CREB expression between diffuse type GCOs with or without recombinant human FBLN5. (I) IF staining for p-CREB expression compared between GCO alone and GCO co-cultured with CAF.

2.2.7. FBLN5 increases cancer aggressiveness in subcutaneous and metastatic xenograft mice models

Spheroid colony formation of MKN-45 and Tcon3944 was

increased in co-culture system of cancer with CAF and FBLN5 knockdown of CAF reversed the tumorigenic effect in the co-culture system. (Figure 6A). In order to investigate the in vivo tumorigenic effect of CAF-derived FBLN5, Tcon3944 xenograft mice model was established and mice were divided into three groups: control group, two groups of cancer and CAF co-implantation, which were subdivided by transfection with shFBLN5 or control vector. Xenograft tumor size were significantly increased when cancer cell was co-implanted with CAFs and knockdown of FBLN5 in CAF diminished tumor growth (Figure 6B). Pathologic exam of extracted xenograft tumors revealed CAF aggravated cancer infiltration into surrounding tissue as well as the expression of EMT markers and inhibition of FBLN5 decreased invasiveness and EMT marker expression (Figure 6C–D). Metastatic gastric cancer mice model created by tail vein injection of Tcon3944 and the effect of CAF coinjection with shScr or shFBLN5 was evaluated. Coinjection of CAF increased number of metastatic lung nodules and expression of EMT marker snail. ShRNA-mediated knockdown of FBLN5 in CAF decreased metastatic lung nodules and snail expression in animal model (Figure 6E–6F). Animal study for in vivo validation showed DGC with CAF shows aggressive feature which was related to CAF originated fibulin-5.

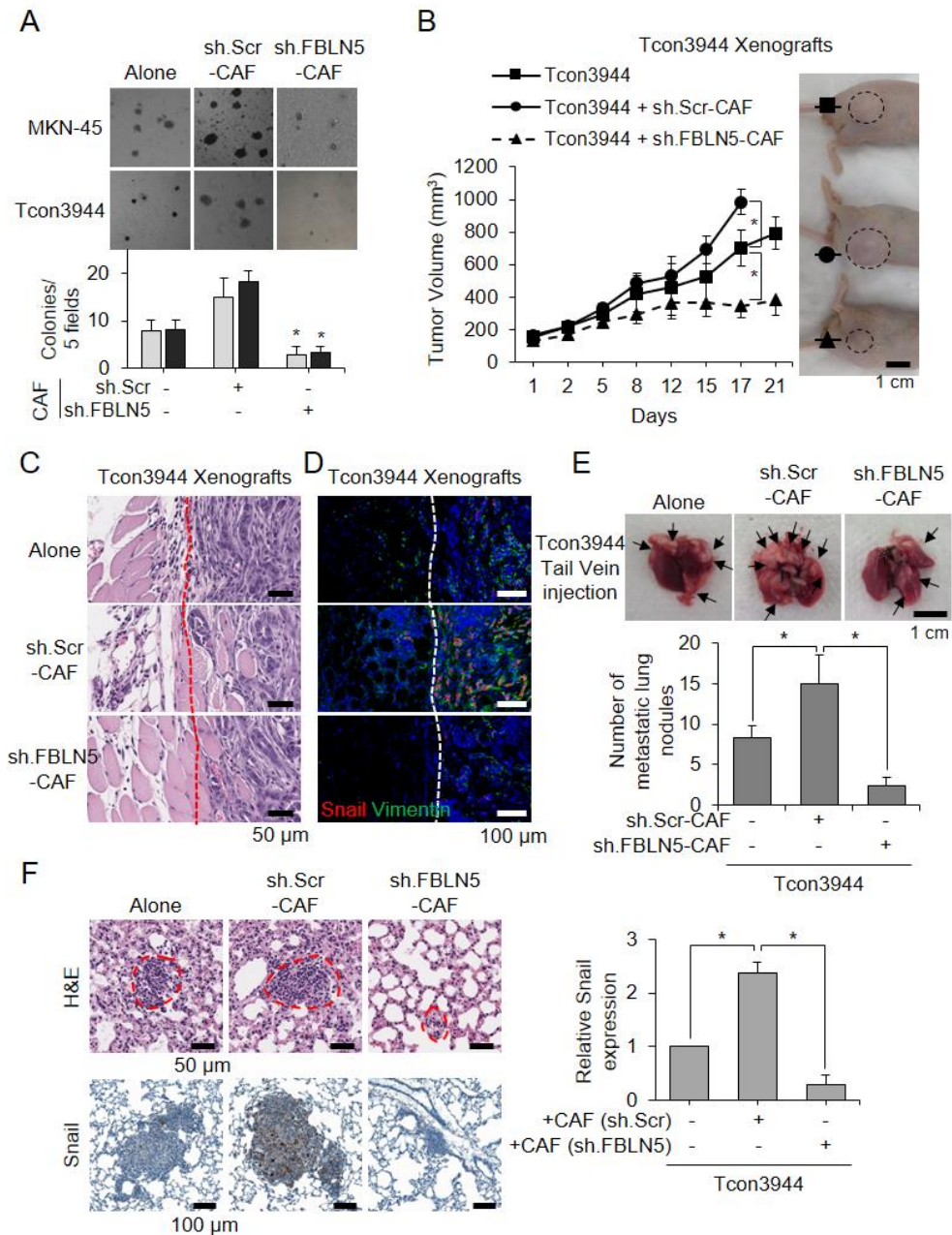


Figure 6. CAF derived fibulin-5 increased aggressiveness of DGC in xenograft mouse models. (A) Colony formation assay for MKN-45 and Tcon3944 cells comparing mono-culture and co-culture system with CAF which can be subdivided by transduction with Sh.Cr or Sh.FBLN5 in CAF. (B) Graphs showing consecutive tumor volume (mm^3) of subcutaneous xenograft mouse models divided by presence of CAF transduced either with sh.Scr. or shFBLN5 along with cancer cells when

injected. Tcon3944 implanted with CAF formed larger volume of subcutaneous tumor compared with single implantation. Tcon3944 co-implanted with CAF knockdown by sh*FBLN5* formed smaller tumor volume. * $P < 0.05$ (C) H&E stain of extracted tumors from three groups of Tcon3944 xenograft mice. Locally advanced invasion of cancer cells around the edge of tumor tissue were more prominent in cancer-CAF co-injected group and sh.*FBLN5* transfected CAF was less likely to exacerbate the invasion of co-injected Tcon3944 to surrounding tissues. Scale bar 50 μ m. (D) Immunofluorescence staining of tumor tissues from mouse xenograft models was performed. Tumor tissue formed from Tcon3944-CAF co-injection protocol showed more prominent EMT marker snail (red) and vimentin (green) expression compared to that of Tcon3944 single injection model. CAF with *FBLN5* knockdown decreased provocation of EMT in co-injected Tcon3944 when co-injected together. Scale bar 100 μ m. (E) Metastatic lung nodules detectable on the surface of the bilateral lungs extracted from metastatic gastric cancer models established by tail vein injection. Metastatic models were divided into three groups depending on the culture system (single Tcon3944 vs CAF co-cultured Tcon3944) and the status of transfection with sh.SCr or sh.*FBLN5* in CAF. Greater numbers of metastatic lung nodules were formed in mice injected with Tcon3944 and CAF together and formation of nodules decreased in mice co-injected with Tcon3944 and *FBLN5* knockdown CAF. Number of metastatic lung nodules of metastatic gastric cancer mice model were shown as bar graphs. (F) Representative image showing H&E stain and IHC for snail of metastatic lung nodules from three groups of metastatic gastric cancer model. Tcon3944 co-injected with CAF formed larger metastatic nodules and showed stronger snail expression compared with Tcon3944 injection alone. *FBLN5* knockdown in co-injected CAF reversed the effect. Relative snail expression of each mice groups of metastasis model were shown as bar graph. * $P < 0.05$

2.3 Discussion

This study identified six differentially activated signaling components between DGC and IGC by mathematical modeling and computer simulation analysis using large scale RNA sequencing data with static statistical approach which reflects dynamic situations among complex molecular networks. Dynamic analysis of large scale RNA sequencing data background is the strong point of our signal network analysis ⁴⁶⁻⁵² Among six DASCs, FBLN5 was verified to have prognostic meaning through tissue TMA from actual patients and detailed clinical information including survival data. Connecting the biological data and clinical finding of actual patients was very important step of our study. Level of FBLN5 expression and survival outcome had strong relationship in DGC patients even after adjustment of confounding variables. This study has the strength to contain vast clinical data of TMA patient sets including survival data which is closely related to actual prognostic significance in patients.

Fibulin-5 was first known for secreted ECM component which has paracrine effect to promote cell adhesions through interaction of integrins and Arg-Gly-Asp (RGD) motif. Fibulin-5 is normally abundant for embryonic development and organogenesis but the defect of it can cause diseases like cutis laxa, Carcot-Marie-Tooth disease and age related macular degeneration ⁵³⁻⁵⁶. Relationship between fibulin-5 and various cancer has been studied but it differed according to the primary sites and whether they are in

positive or negative correlation is still controversial^{33,35,36,41,57-60}. In some cancers, fibulin-5 even acted as a tumor suppressor depending on the balance between the inhibition of angiogenesis and tumor promoting effect on cancer cells^{32,61}. However, in gastric cancer study, high fibulin-5 was related with more malignant features including poor differentiation, lymph node metastasis and advanced TNM stage^{42,62}. Our study result made up for more detailed clinical information and survival data, which also showed worse prognostic effect of fibulin-5 consistent with previous study.

This experimental study found out fibulin-5 was secreted from CAF in DGC, having paracrine effect of promoting cancer cell invasion and metastasis through advanced EMT. Knockdown of FBLN5 with transfection of shFBLN5 decreased invasion, metastasis and EMT marker expressions of DGC cells. Treatment with recombinant human fibulin-5 increased the number of organoids over 50 μ m in size and fibulin-5 was even detectable in patient's plasma, which shows possibility of systemic effect of fibulin-5 in addition to local paracrine effect in TME. In vivo study with xenograft mice model including subcutaneous injection model or tail vein injection model showed consistent correlation between high fibulin-5 and increased tumor aggressiveness including increased size, more invasion, high EMT marker and more metastasis. Probable downstream pathway of secreted fibulin-5 in cancer cell is CREB-GSK-3 α pathway according to the result of phosphokinase array and other supporting experiments. CREB overexpression is influenced by numerous different mechanisms

and is related to cancer migration, metastasis and poor survival in many cancers, thus, CREB inhibition was thought to be a promising therapeutic target⁶³⁻⁶⁶. For the first time, we investigated fibulin-5 as a CREB regulator in DGC and fibulin-5 inhibitor can be a promising treatment target of DGC with the effect of subsequent CREB inhibition. Knockdown of shFBLN5 eventually decreased activation of CREB and CREB inhibitor mimicked the effect of FBLN5 inhibition, which showed close correlation between those two factors. Limitation of this study is that we couldn't explain exact mechanism of the fibulin-5 activating CREB/GSK-3 α pathway which finally results in cancer progression by EMT increase of DGC but probable theoretical hypothesis is that fibulin-5 binds to integrins of cancer cell and activates downstream CREB pathways^{67, 62, 68-71}. Further experimental study is needed to better understand the exact mechanism. Furthermore, considering the role of FBLN5 in each different cancers is controversial and different in context-dependent manner, substantial follow up studies are needed in gastric cancer to confirm the tumor progressive role of FBLN5 in gastric cancer.

Chapter 3. Conclusion

Fibulin-5 is one of differentially activated signaling components between intestinal and diffuse type gastric cancers. Fibulin-5 is derived from cancer-associated fibroblast and this can affect epithelial-mesenchymal transition of the diffuse gastric cancer cell via c-AMP responsive element-binding protein pathway. Finally, fibulin-5 increases aggressiveness of diffuse gastric cancer cell and survival of the patients becomes worse. Further studies are needed to understand the exact mechanism of fibulin-5 and invent the future drug targeting fibulin-5.

Bibliography

국문초록

미만형 위암은 섬유화된 간질과 저응집세포로 이루어져 있고 예후가 나쁘다. TCGA, GSE62254, GSE26253 세가지 RNA 시퀀싱 유전자 데이터를 사용한 대규모 신호망분석을 통하여 장형 위암에 비해 미만형 위암에서 FBLN5 유전자가 높은 활성도를 보임을 확인하였으며 실제 미만형 환자의 임상정보 및 조직유전자 미세배열을 사용한 면역화학염색을 통해 높은 FBLN5 발현이 나쁜 예후와 연관이 있다는 것을 확인하였다. 피블린5 단백질은 섬유화 간질에 있는 암연관 섬유아세포에서 기원하여 미만형 암세포와 함께 배양하였을 때 미만형 암세포의 상피간질전환을 증가시켜 암세포의 이동과 침윤을 증가시켰다. 이러한 피블린5 단백질의 영향은 c-AMP 반응성 요소 결합 단백질 경로를 통해 작용한다. 암연관 섬유아세포의 FBLN5 유전자 발현을 억제하면 미만형 위암세포에서 c-AMP 반응성 요소 결합 단백질 유전자를 억제하거나 억제화합물질을 사용할 때와 같이 암의 공격성이 감소함을 확인하였다. 이종이식 마우스 모델을 사용한 생체 내 실험에서 미만형 위암이 암연관 섬유아세포와 같이 주입되었을 때 생착된 종양의 크기가 크고 공격성이 증가함을 확인하였고 이러한 효과는 FBLN5 유전자를 억제하면 감소하였다. 이로써 FBLN5 단백질이 미만형 위암에서 중요한 예후인자가 될 수 있음을 확인하였다.

주요어 : 미만형 위암, 암연관 섬유아세포, FBLN5, 피블린-5, 상피간엽전환

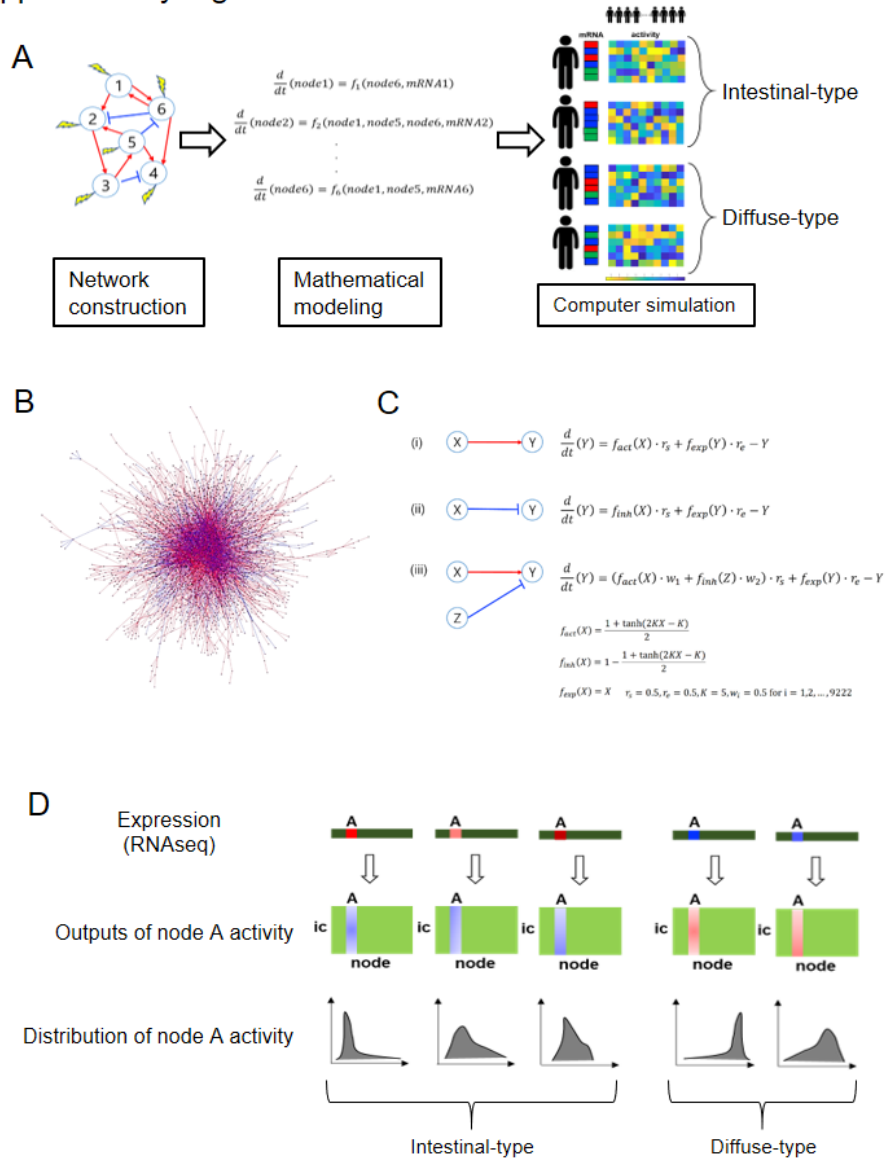
학번 : 2019-38342

Supplements

Supplementary Fig. 1 Whole analysis flow of reconstructed large-scale

signaling network study (A) Analysis scheme for the large-scale cancer signaling network. Step 1) Construct a large-scale cardiac signaling network; Step 2) Formulate the network as a mathematical model using the normalized equation modeling method and conduct the numerical simulation using ode15s function in MATLAB; Step 3) Compare the activity of signaling components between intestinal type and diffuse type tumors. (B) The network consists of 3557 nodes and 8509 links. Each dot represents the node and each line represents the link (red line for activation link and blue line for inhibition link). The network is reconstructed based on SIGNOR database (<https://signor.uniroma2.it>) (C) Formulations for the mathematical model: (i) the formulation for the link, “X activates Y”; (ii) the formulation for the link, “X inhibits Y”; (iii) the formulation for the link, “X activates Y and Z inhibits Y”. (D) The process of finding out DASCs; Simulation of the mathematical model using processed RNA sequencing data result in the distribution of activity of the signaling components. Since one million simulations were performed using one million different initial conditions, one million values for each signaling components finally come out and can be represented as a form of distribution. By comparison of the distributions, DASCs can be investigated.

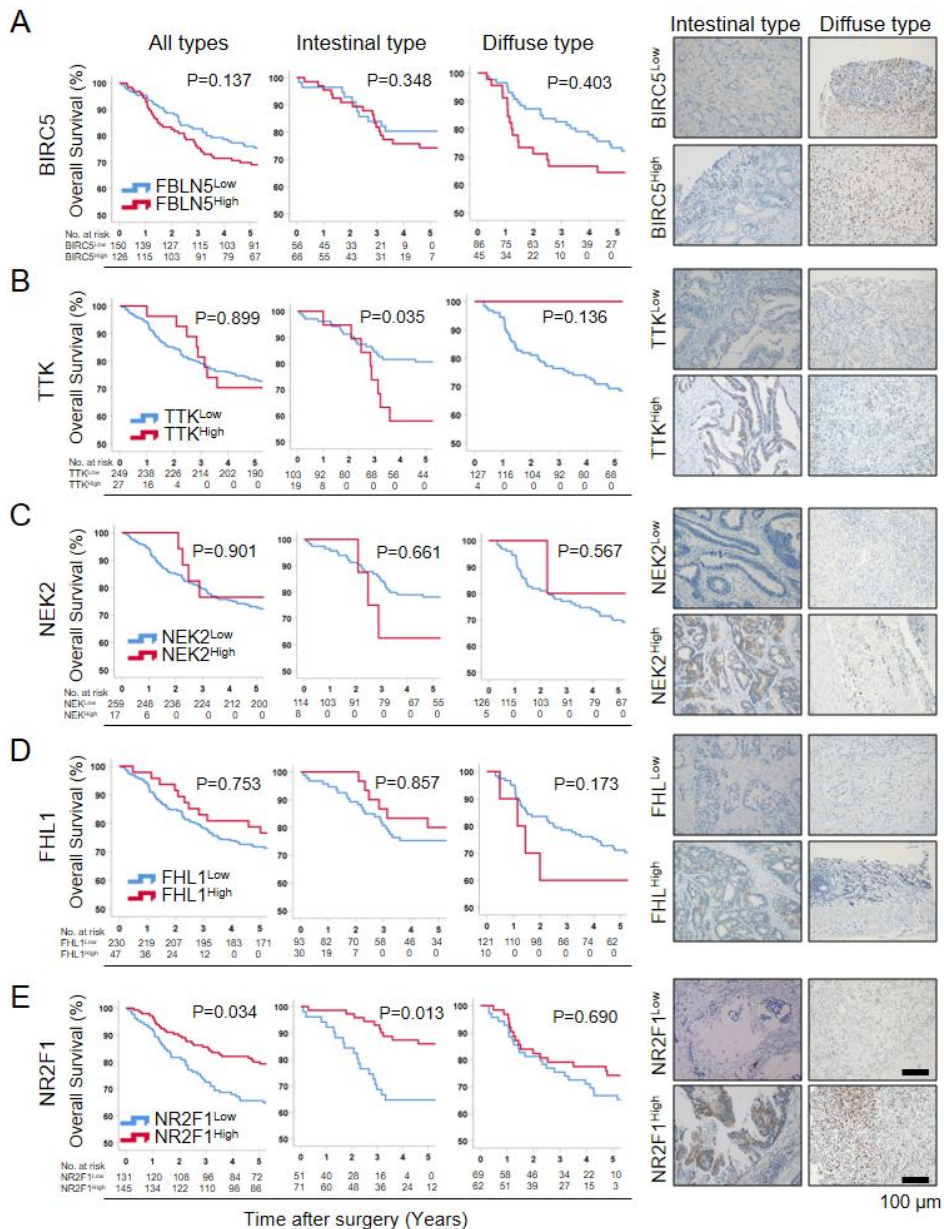
Supplementary Figure S1



Supplementary Fig. 2. Overall survival analysis and immunohistochemical staining of TMA blocks of gastric cancer patients included in clinical validation cohort. Overall survival (OS) was compared between patient groups divided by the expression level five differentially activated signaling components (DASCs) found by signaling network analysis in addition to FBLN5. Each OS was evaluated in total patients and in subgroups divided by Lauren types. Paired IHC staining of TMA blocks of the patients was shown in the right side of each OS

graphs containing representative low and high expression patterns of DASCs expression compared between intestinal and diffuse type gastric cancers. (A) BIRC5 (B) TTK (C) NEK2 (D) FHL1 (E) NR2F1. Scale bar 100 μ m.

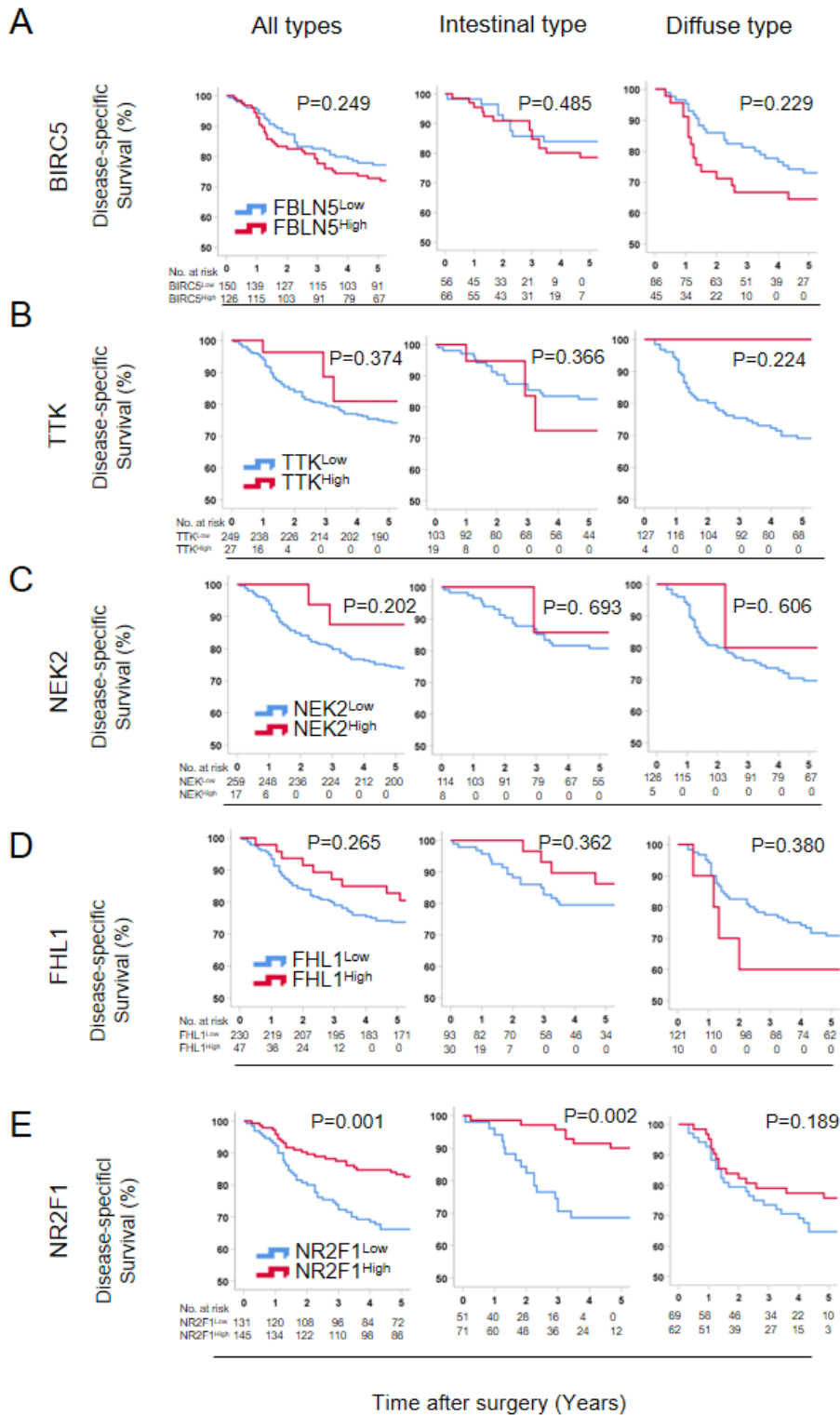
Supplementary Figure S2



Supplementary Fig. 3. Disease-specific survival analysis of gastric cancer patients included in clinical validation cohort. Disease-specific survival (DSS)

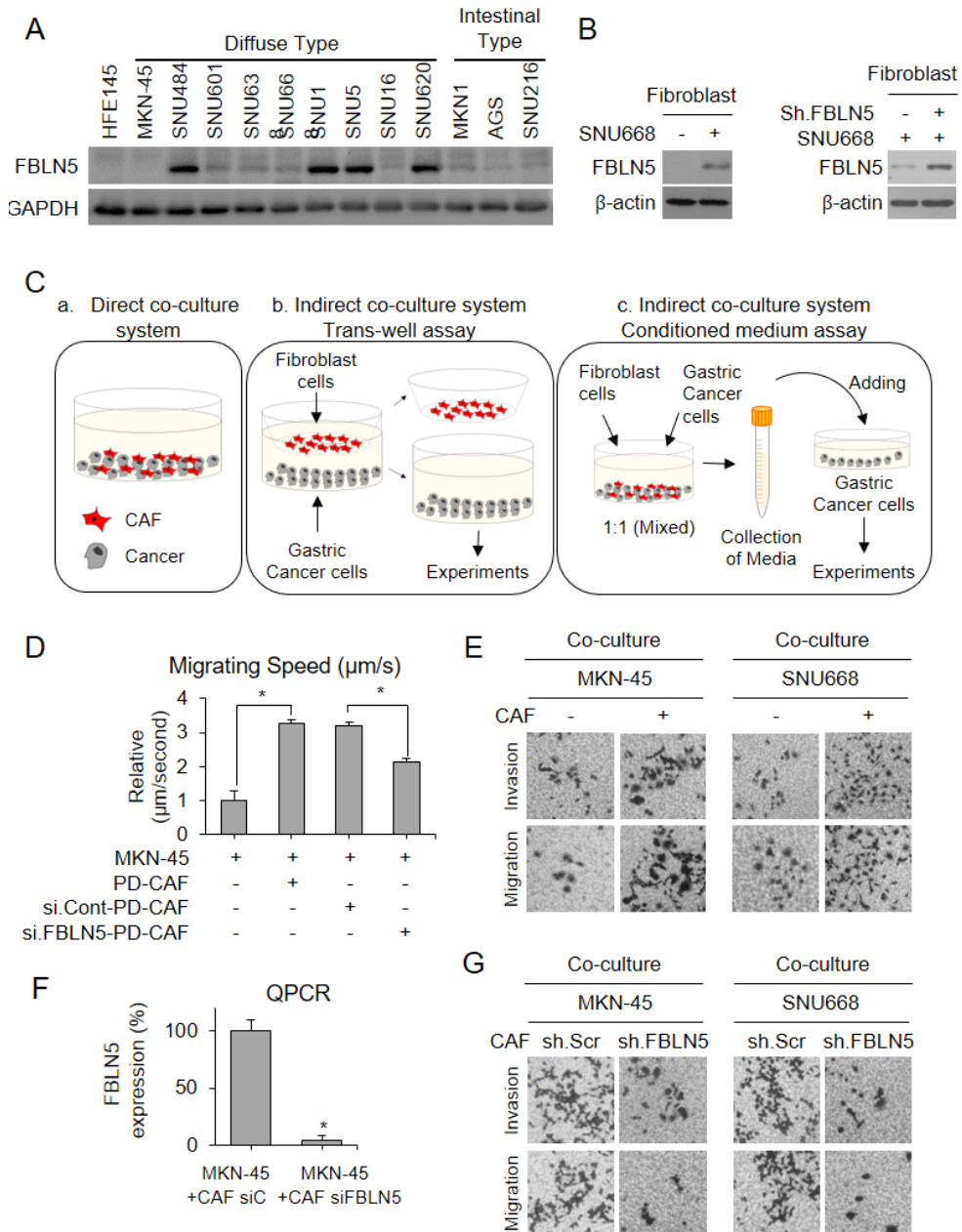
was compared between patient groups divided by the expression level of five differentially activated signaling components (DASCs) found by signaling network analysis. Each DSS was evaluated in total patients and in subgroups divided by Lauren types.

Supplementary Figure S3



Supplementary Fig. 4. FBLN5 level of gastric cancer cell lines was screened followed by adopting cancer cell line plus cancer-associated fibroblast (CAF) co-culture system (A) Expression level of FBLN5 was screened in variable gastric cancer cell lines ahead of the in vitro cell study. MKN45 and SNU668 diffuse gastric cancer cell lines with low FBLN5 were chosen to investigate the role of CAF-derived fibulin-5. (B) Expression level of FBLN5 in fibroblast was compared between fibroblast alone and fibroblast with SNU668 co-culture. Transfection of *shFBLN5* in fibroblast showed effective knockdown of FBLN5 expression in fibroblast. (C) Comprehensive figures showing three methods of co-culture consisted of diffuse gastric cancer cell line and CAF used in this study. (D) Migration speed of MKN45 analyzed by Operetta live cell imaging system was compared according to the presence of patient-derived CAF (PD-CAF) and whether or not PD-CAF FBLN5 was knockdown by si-FBLN5. Bars represent average speed of MKN45 ($\mu\text{m/s}$) and standard deviation. (E) Cancer cell migration and invasion assays using MKN-45 or SNU668 to investigate the difference of cancer cell plus CAF co-culture system compared with cancer cell mono-culture system. (F) Quantitative PCR analysis for FBLN5 expression in CAF to investigate the effect of FBLN5 knockdown by siRNA in CAF which consists of cancer cell plus CAF co-culture system. (G) Cancer cell migration and invasion assays using MKN-45 or SNU668 in co-culture system compared by FBLN5 knockdown status in CAF included in co-culture system.

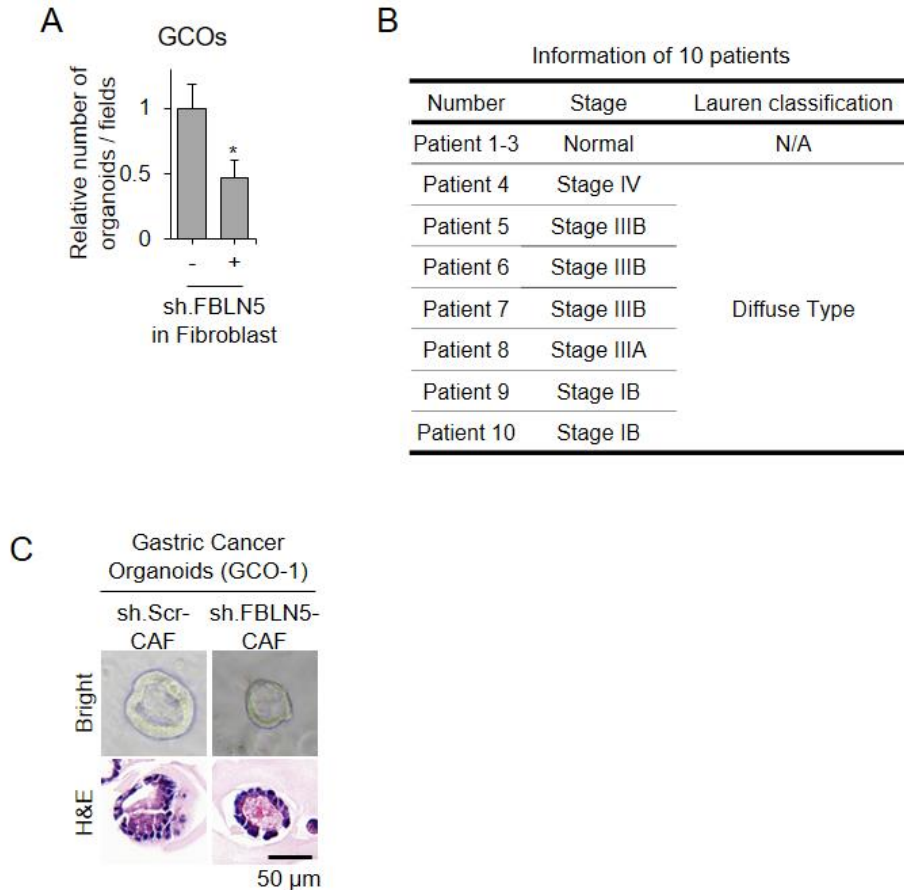
Supplementary Figure S4



Supplementary Fig. 5. (A) Comparison of relative number of organoid in co-culture system by the FBLN5 knockdown status in fibroblast. (B) Brief clinical information of 10 patients whose blood samples were used in ELISA test to detect plasma fibulin-5. (C) Comparison of bright-field microscopic image of GCOs and number of GCOs with size greater than $50 \mu\text{m}$ between three organoid groups; GCO alone, GCOs co-cultured with CAF transfected shScr, GCOs co-cultured with

CAF transfected with sh*FBLN5*

Supplementary Figure S5



Supplementary Fig. 6. Experiments showing the possible relations between fibulin-5 and c-AMP response element binding protein (CREB) (A) Western blots for phospho-RSK-1, RSK-1/2/3 and HSP60 compared between MKN45 monoculture system and MKN45-CAF co-culture system. (B) Western blots showing the change of expression level of CREB (pCREB Ser133) and GSK-3 α (pGSK-3 α Ser21) in co-culture system of each cancer cell (MKN45, SNU668) with CAF under the influence of CREB inhibitor 666-15. (C) Western blots showing the difference of EMT markers (N-cadherin, Vimentin, Snail, Slug) after treatment of 666-15 in co-culture system of MKN-45 or SNU668 with CAF. (D) Migration and invasion assay to investigate the effect of CREB inhibition in Cancer-CAF co-

culture system. Relative positive cells in each study were shown as bar graph. * $P < 0.05$ (E) Migration and invasion assay to investigate the effect of CREB knockdown of cancer cell lines included in Cancer-CAF co-culture system.

Supplementary Figure S6

